Coordination Chemistry Reviews 255 (2011) 2401–2425

Contents lists available at ScienceDirect

Coordination Chemistry Reviews

journal homepage: www.elsevier.com/locate/ccr

Review

Light-emitting devices based on organometallic platinum complexes as emitters

Jan Kalinowski[a,1], Valeria Fattori[b,*], Massimo Cocchi[b], J.A. Gareth Williams[c,**]

[a] Gdańsk University of Technology, 80-233 Gdańsk, Poland
[b] Institute of Organic Synthesis and Photoreactivity, National Research Council of Italy (ISOF-CNR), 40129 Bologna, Italy
[c] Department of Chemistry, University of Durham, Durham DH1 3LE, UK

Contents

ARTICLE INFO

Article history:
Received 15 October 2010
Accepted 26 January 2011
Available online 5 March 2011

Keywords:
Platinum complexes
Cyclometallation
Luminescence
Electroluminescence
OLEDs
Optical switches

ABSTRACT

This article provides an overview of molecular optoelectronic systems – particularly organic light emitting devices (OLEDs) – that make use of platinum(II) complexes as their emissive components. A comprehensive introduction to the function and classes of OLEDs in general is first provided. The diverse range of parameters that are used to quantify OLED performance can be bewildering, particularly to the chemist, and we set out the relationship between the key parameters, and provide a detailed description of the main physical processes that determine them. We then focus on OLEDs prepared using platinum(II) complexes as dopants. Pertinent recent developments in the chemistry of luminescent Pt(II) complexes containing cyclometallating bidentate and terdentate ligands are presented. Some of these complexes possess outstanding features from the point of view of their electronic structure, photophysical behaviour, processability, and environmental stability. An appreciation of the nature of their molecular excited states has facilitated understanding of the fundamental electronic processes at work within devices, and has led to the fabrication of high-performance OLEDs. In addition to single-colour and white light systems, some of them offer unusual characteristics and applications, such as plant growth OLED (PGOLED) or electro-photoluminescent (EL-PL) switches. Such devices fulfil the requirements to become an important part of 'Green Photonics'.

© 2011 Elsevier B.V. All rights reserved.

1. Introduction and scope

The general message of the present review is inspired by the goals of "Green Photonics"—optoelectronics that enables many aspects of the green revolution [1]. It is finding a common interest in reducing energy consumption in such diverse markets as optical communication components, light-emitting diodes (LEDs),

* Corresponding author. Tel.: +39 051 639 9809; fax: +39 051 639 9844.
** Corresponding author. Tel.: +44 0 191 33 42124.
E-mail addresses: fattori@isof.cnr.it (V. Fattori), j.a.g.williams@durham.ac.uk (J.A.G. Williams).
[1] Deceased 18th December 2010.

0010-8545/$ – see front matter © 2011 Elsevier B.V. All rights reserved.
doi:10.1016/j.ccr.2011.01.049

solid-state lighting and solar photovoltaic cells. From solar and solid-state lighting, to optoelectronics used in manufacturing and metrology for green products, optoelectronics enables or provides technology that reduces power, waste and pollution. Among this plethora of applications, organic LEDs (OLEDs) are envisaged as playing a major role in the area of flat panel (RGB) displays, as well as offering novel lighting sources that are less expensive and more efficient than conventional incandescent and fluorescent illumination sources [2].

In contrast to their inorganic semiconductor counterparts, OLEDs rely on electroluminescence (EL) from excited-state organic molecules to generate light. By tailoring the composition of the organic material, it is possible to create devices that emit red, green, blue, or collectively white light when electrically driven. Today's state-of-the-art phosphorescent organic light emitting devices (PHOLEDs) are able to offer efficiencies of 60 lm/W at 1000 cd/m^2 and, in the case of white light systems, high colour-rendering indexes (CRI) reaching 90. Recently, improving PHOLED technology enabled to break through the 100 lm/W value [3]. To date, PHOLEDs with active areas up to 25 cm^2 and 0.7 mm thick have been reported [4], while highly conductive organic materials allow the operating voltage to be kept below 4 V. An LT50 index (the time taken for light output to decrease by 50% when the device is driven at a constant current) of 10,000 h has been achieved on the laboratory scale (2 mm^2) for warm-white light OLEDs (WOLEDs) with an initial luminance of 1000 cd/m^2. This level of performance makes PHOLEDs very attractive for niche lighting applications such as night lights.

Despite such recent progress, there is still a significant amount of work to be done before high-efficacy OLEDs become a commercial reality. A variety of challenges to reach this goal can be identified. Many of them relate to synthesis and selecting organic materials and device architectures for low-cost manufacturing of high-efficiency OLEDs. Of the various classes of organic emitters, cyclometallated platinum complexes appear to be of particular interest since they reveal high quantum phosphorescence efficiency at room temperature, utilizing effectively both singlet and triplet excited states in the radiative processes within the OLED's emitting layers (EMLs). The strong spin-orbit coupling of the platinum atom allows for efficient intersystem crossing (ISC) between singlet and triplet states, which can lead to a high quantum yield of emission from the triplet state. The excited states of Pt(II) complexes can now be readily tuned to emit with high efficiency throughout the visible and near-infrared (NIR) regions of the spectrum, their emission characteristics being governed by the nature of the ligand and the extent of mixing of its molecular orbitals with the atomic orbitals of the metal ion. For example, the formally forbidden radiative relaxation of $^3\pi$–π^* transitions is promoted by mixing with ^{1}MLCT (singlet metal-to-ligand charge-transfer) states, leading to quantum efficiencies of triplet state emission now approaching unity at room temperature [5].

Such behaviour is, of course, not unique to platinum(II). Indeed, complexes of its neighbour in the periodic table, iridium(III), a d^6 metal ion, have been far more widely explored as OLED emitters. However, d^8 Pt(II) complexes are attractive for another reason. Their square-planar structures allow them to interact facially with one another. They may aggregate through attractive intermolecular interactions of Pt–Pt or ligand–ligand or a combination of these, thereby facilitating formation of bi-molecular (B-M) states, either in the ground state (dimers) or exclusively in the excited state (excimers and electromers). Efficient simultaneous emissions from B-M and mono-molecular (M-M) excited states can lead to broad coverage of the visible spectrum and to white light generation with a single dopant [5,6].

In this review, recent efforts to develop a deeper insight into the parameters that are important in optimizing the performance of Pt-based PHOLEDs are described. As part of continuing studies of electrophosphorescence, we report on current investigations of a selection of recently developed phosphorescent platinum complexes with terdentate, cyclometallating ligands. With judicious choices of dopant and materials, it has proved possible to make various types of efficient OLEDs, having diverse colours and varying performance parameters designed for different applications. Their recent highlights will be presented in some detail, following an overview of the general function and architectures of the various sorts of OLEDs and an outline of the chemistry of cyclometallated platinum(II) complexes. A comprehensive introduction to OLEDs forms an integral part of the review, in order to facilitate the description and understanding of the merits of the devices presented within a single, self-contained article, without requiring the reader to refer to separate OLED monographs.

2. Introduction to organic light-emitting diodes (OLEDs)

2.1. Definition and general device architecture

The commonly accepted notion of an OLED is a thin organic film device exploiting charge-recombination electroluminescence (REL) [7]. In thin-film OLEDs, electrons are injected from a cathode, usually a metal with a low work function like Mg, Al, Ca, and holes are injected from an anode, usually a transparent layer of indium-tin-oxide (ITO). Under an applied electric field, the carriers approach one another in the emitting layer (EML) of the device. If both charges arrive on a single molecule or, more generally, on a pair of closely spaced molecules, single-molecule or two-molecules-underlain excited states may be formed [8–10]. Their radiative decay produces EL light (Fig. 1). The EL is generated within the weak cavity formed by the highly reflective top metal electrode and a less reflective ITO/glass interface. The EL can be transferred to the externally radiated modes, or to the waveguide side modes propagating within the plane of the layers forming the device structure. Furthermore, a fraction of the EL radiation is lost to the metal cathode via non-radiative dipole–metal transfer, and excitation of surface plasmons; the other fraction being reflected at the cathode can contribute either to external or side radiated modes.

2.2. Performance characteristics

The most important critical figures of merit for organic LEDs are the energy conversion efficiency (η) and the quantum EL efficiency (φ_{EL})

$$\eta = \frac{\Phi_R}{Ui}, \qquad \varphi_{EL} = \frac{e\Phi_{EL}}{j} = \frac{eU}{h\nu}\eta(\text{photon/carrier}) \tag{1}$$

Here, Φ_R is the light-energy (radiant) flux (in watts), Ui is the electrical power, e is the electron charge, Φ_{EL} is the EL quantal ($h\nu$) flux per unit area (A), $j = di/dA$ is the current (i) density and U is the voltage applied to the LED. For face-detected emission (as is usually the case, see Fig. 1), only a certain fraction of the light generated in the EML is available for front detection because a large fraction of the emitted light is lost to waveguiding modes in the glass, ITO, and organic layers due to refractive index (n) mismatching. These losses make the measured (external) $\varphi_{EL}^{(ext)} = \xi\varphi_{EL}$ considerably lower than φ_{EL} (see Fig. 1). The LED structure dependent quantity $\xi = (1-R)(1-\cos\Theta_c)\exp(-\alpha x) < 1$, accounting for the overall losses, is called the "light output coupling factor". It takes into account the self-absorption loss $\exp(-\alpha x)$, where α is the linear absorption coefficient. The interface effects due to reflectance, R, and $\Theta_c = \arcsin(n^{-1})$, are apparently influenced by the optical constants of the LED components, including those of the EMLs.

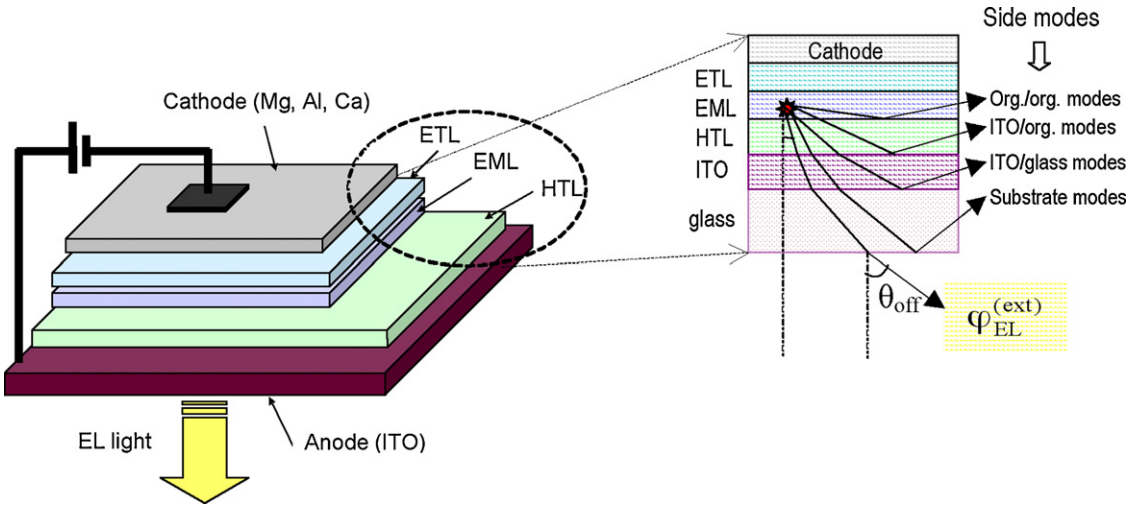

Fig. 1. Fundamental architecture of a three-layer OLED (left) along with the various radiative modes generated within this archetypal device structure (right): ETL, organic electron-transporting layer; EML (~30–100 nm), light emitting layer (emitter); HTL, organic hole-transporting layer; ITO, inorganic indium tin oxide layer serving as the conducting anode and a transparent window for near UV, visible and near IR radiation. The side modes are generated within the microcavity as a result of the total internal reflection at various interfaces: air/glass (substrate) modes, ITO/glass modes, ITO/org. (ITO/organic HTL) modes, org./org. (organic ETL/organic HTL) modes.

One would expect the factor ξ, and thus $\varphi_{EL}^{(ext)}$, to decrease with increasing refractive index, n, of the organic materials used in the fabrication of the OLED.

A recently proposed unified approach defines the external EL quantum efficiency (ELQE) of OLEDs by taking into account all the electronic processes involved in the creation and fate of n different excited states, modified by the phosphor concentration, c, in EMLs [11]:

$$\varphi_{EL}^{(ext)}(c) = P_R(c)P_d\sum_{i=1}^{n}\xi_i(c)\varphi_i^{PL}(c)P_{qi}(c)P_{si} \quad (2)$$

Here, $\xi_i\,(c)$ (<1) is the light output coupling factor described above and dependent on the LED's material composition, architecture and operation conditions, and φ_i^{PL} is the quantum efficiency of the radiative decay of excited state i created in the electron-hole recombination process, which is commonly identified with the photoluminescence (PL) quantum efficiency. The fundamental message of Eq. (2) is that the ELQE is a result of the superposition of four independent processes operating in the LED at the same time, represented by the factors

$$P_R = \left(1+\frac{\tau_r}{\tau_t}\right)^{-1}, \quad P_d = \left(1+\frac{\tau_c}{\tau_d}\right)^{-1},$$

$$P_{qi} = \left(1+\frac{\tau_{0i}}{\tau}\right)^{-1}, 0 \le P_{si} \le 1, \quad (3)$$

which account for the probability of the formation of a charge-pair (CP) state (P_R), its dissociation avoidance (P_d), and escape of a quenching process by the final emissive i state (P_{qi}), irrespective of the type of emissive material and LED architecture. The P_{si} stands for the probability of creation of a singlet or triplet ith emitting state. They are defined by spin multiplicity and a set of time constants characterizing the formation and decay of various electronic species as depicted in the scheme presented in Fig. 2. These are: the charge carriers' encounter (recombination) time (τ_r); the effective transit time of charges out of the recombination zone (τ_t), corresponding to the maximum of the monomolecular decay rate constant of electrons $(\tau_t^e)^{-1}$ and holes $(\tau_t^h)^{-1}$, $(\tau_t)^{-1} = (\tau_t^e)^{-1} + (\tau_t^h)^{-1}$; the dissociation time of CP states (τ_d); the formation time of an emissive state (T_1)≡charge-pair internal capture time (τ_c); the intrinsic lifetime of the emissive state (τ_0) and its lifetime (τ) triggered off by exciton–exciton ($T_1 + T_1$) and exciton–charge carrier interactions (T_1 + e and/or h).

Another important factor characterizing an OLED is luminous efficacy, which is defined by the ratio of the luminous flux as detected by the human eye, to power. Depending on the context, the power can be either the radiant flux of the source's output, or it can be the total electric power consumed by the source. Which sense of the term is intended must usually be inferred from the context, and is sometimes unclear. The former sense is sometimes called luminous efficacy of radiation (LER), and the latter luminous efficacy of a source (LES) or the overall luminous efficacy. The LES describes how well the source provides visible light from a given amount of electricity. The LER is a characteristic of a given spectrum that describes how sensitive the human eye is to the mix of wavelengths involved. The luminous efficacy of a source is the LER of its emission spectrum times the conversion efficiency from electrical energy to electromagnetic radiation denoted in (1) by η. The overall luminous efficacy is a measure of the efficiency of the device with the output adjusted to account for the spectral response curve (the "photopic luminosity function"). When expressed in dimensionless form (for example, as a fraction of the maximum possible luminous efficacy), this value may be called overall luminous efficiency, or simply the lighting efficiency. Because the eye response varies across the visible spectrum, a specific unit, the lumen (lm), is defined to quantify perceived luminous intensity. The lumen is defined as the amount of light given into one steradian (sr) by a point source of one candela strength; while the candela, a base SI unit, is defined as the luminous intensity of a source of monochromatic radiation, of wavelength 555 nm, and a radiant intensity of 1/683 W per steradian. The number 1/683 was chosen to make the candela about equal to the standard candle, the unit which it superseded. By definition, a typical human eye has a maximum luminous sensitivity corresponding to the LER = K_{max} = 683 lm/W at a wavelength λ = 555 nm. Response in the blue and red is much weaker and the wavelength dependence of $K(\lambda)$ for the human eye is given by the so-called 'photopic response' curve $V(\lambda) = K(\lambda)/K_{max}$ with a V_{max} (555 nm) = 1 at 555 nm (see e.g. Refs. [12,13]). Since the 'photopic response' is a function of the wavelength (λ) of light, the conversion from radiometric units to photometric units first requires knowledge of the spectral profile of the light source. If the source is specified as having a certain colour temperature, we can assume that its spectral radiance emittance is the same as a perfect

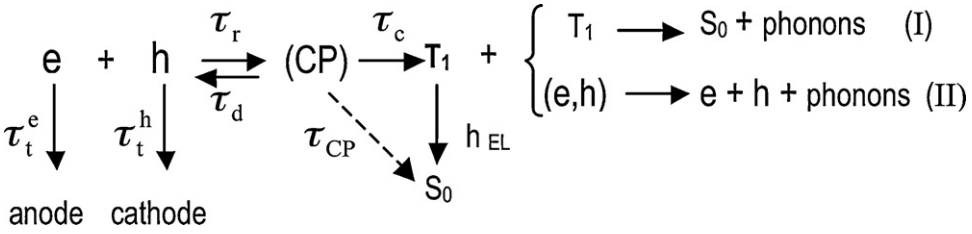

Fig. 2. The kinetic scheme illustrating formation of emissive states (T_1) in the recombination process of electrons and holes injected at the electrical contacts (e + h). Naturally, the emissive state is preceded by an intermediate state of a coulombically correlated charge pair (CP). In general, CP can also directly decay to the ground molecular state (S_0) either in a radiative or radiationless transition with a time constant τ_{CP}. The radiative decay of T_1 produces the only optical emission called electroluminescence ($h\nu_{EL}$) if τ_{CP} is much longer than charge capture time (τ_c). For description of other time constants, see text. The yield of the radiative decay can be reduced by ($T_1 + T_1$) (I) and (T_1 + e and/or h) (II) interactions. Here the emissive state (T_1) stands for either the first monomolecular triplet exciton or excimer triplet state, and factor $P_{si} = 1$ ($P_{s1} = P_{s2}$) since, due to the heavy Pt atom, strong spin-orbit coupling transforms all singlet states into triplets.

black body radiator and use Planck's Law. Integration of the product of the light emittance by the photopic function provides the conversion from a radiometric signal to a photometric unit. The conversion between photometric units which takes into account human physiology and straight radiometric units is given by the following: (photometric unit) = (radiometric unit) × K_{max} × $V(\lambda)$ and basically tells us how efficiently the eye picks up certain wavelengths of light. The photopic response, Φ, of the eye to incident light with an arbitrary spectrum $\varphi(\lambda)$ can be calculated using Eq. (4),

$$\Phi = \frac{\int_0^\infty \varphi(\lambda)V(\lambda)K_{max}d\lambda}{\int_0^\infty \varphi(\lambda)d\lambda} \quad (4)$$

where $\int_0^\infty \varphi(\lambda)V(\lambda)K_{max}d\lambda = \Phi_L$ calculates the total luminous flux (or visible energy) in lumens and $\int_0^\infty \varphi(\lambda)d\lambda = \Phi_R$ the total radiant flux in watts for a source of light. The luminous intensity (I_L) and radiant intensity (I_R) are obtained by dividing a luminous and a radiant flux by solid angle and measured in lumens per steradian (lm/sr) or candela (cd) (1 cd = 1 lm/sr) and radiant intensity (I_R) measured in W/sr, respectively. The I_R and I_L divided by the emitting area define radiance, R (W/sr × m^2), and luminance, L (lm/sr × m^2 or cd/m^2), respectively. The power efficiency (PE) is defined by the ratio $\eta_P = \Phi_L/Ui$ of the luminous flux, Φ_L, and the electrical power consumed in the device Ui, where i is the current and U applied voltage. The power efficiency is directly related to the quantum efficiency (1) through Eq. (5)

$$\eta_P = \frac{h\nu}{eU}\Phi\varphi_{EL}(\mathrm{lm/W}) \quad (5)$$

Though the dimension of η_P is identical to that of Φ, these quantities are by no means equivalent. Whereas, Φ characterizes the visual response (lm) of the eye to the energy of the radiant light flux (W), the η_P characterizes the light source providing the emitted luminous flux (lm) per unity of the electric power (W) consumed by the device.

Of practical use is the current or luminous efficiency (LE) of OLEDs defined as the luminous intensity from the device measured in candelas relative to the driving current, thus measured in (cd/A). We note that because of the summation over the visual portion of the electromagnetic spectrum that is part of this weighting, the unit of "lumen" is colour-blind: there is no way to tell what "colour" a lumen will appear. The human eye has photoreceptors for medium- and high-brightness colour vision, with sensitivity peaks at short (S, 420–440 nm), middle (M, 530–540 nm), and long (L, 560–580 nm) wavelengths (there is also the low-brightness monochromatic "night-vision" receptor, called rod cell, with peak sensitivity at 490–495 nm). Thus, in principle, three parameters describe a colour sensation. The tristimulus values of a colour are the amounts of three primary colours in a three-component additive colour model needed to match that test colour. The tristimulus values are most often given in the CIE (the Commission Internationale de L'Eclairage) 1931 colour space, in which they are denoted X, Y, and Z (see Fig. 3a) [14]. Chromaticity coordinates, also known as CIE coordinates, ($\bar{x}$, $\bar{y}$), are defined by calculating the tristimulus response of the colour-respective parameters, i.e.:

$$\begin{aligned} x &= \int_0^\infty \varphi(\lambda)X(\lambda)d\lambda \\ y &= \int_0^\infty \varphi(\lambda)Y(\lambda)d\lambda \\ z &= \int_0^\infty \varphi(\lambda)Z(\lambda)d\lambda \\ \bar{x} &= \frac{x}{x+y+z} \\ \bar{y} &= \frac{y}{x+y+z} \end{aligned} \quad (6)$$

where $X(\lambda)$, $Y(\lambda)$, and $Z(\lambda)$ are the responsivities of the three receptors. The ($\bar{x}$, $\bar{y}$) coordinates can be plotted on a colour chart such as Fig. 3b. Any specific method for associating tristimulus values with each colour is called a colour space. CIE XYZ, one of many such spaces, is a commonly used standard, and serves as the basis from which many other colour spaces are defined.

After colour, the most important aspect determining the illumination quality of an OLED is its colour rendition, i.e., how "true" different coloured objects appear when illuminated by the OLED and how well subtle variations in colour shades are revealed. This is described by Colour Rendering Index (CRI), expressed as a rating from 0 to 100. The higher the CRI rating, the better its colour rendering ability. Note that the CRI by itself does not indicate what the colour temperature of the reference light source is; therefore, it is customary also to cite the correlated colour temperature (CCT). The colour temperature of a light source is the temperature of an ideal black-body radiator that radiates light of comparable hue to that light source. The CRI is calculated by comparing the colour rendering of the test source to that of a "perfect" black body radiator for sources with correlated colour temperatures under 5000 K, and a phase of daylight otherwise (e.g. CIE standard colour illuminant D65 with the CIE 1931 colour space chromaticity coordinates of $x = 0.31$, $y = 0.32$ using the standard observer and $x = 0.31$, $y = 0.33$ using the supplementary observer. Since D65 represents white light, its co-ordinates are also a white point, corresponding to a correlated colour temperature of 6504 K [15]).

2.3. Mechanisms of electroluminescence (EL) and operation modes of OLEDs

The general EL phenomena can be classified according to criteria based on three fundamental processes: (a) electrical energy supply, (b) excitation mode of emitting states, and (c) the light generation mechanism itself [7,8,16]. Of the various types of organic EL which are often distinguished on the basis of excitation modes,

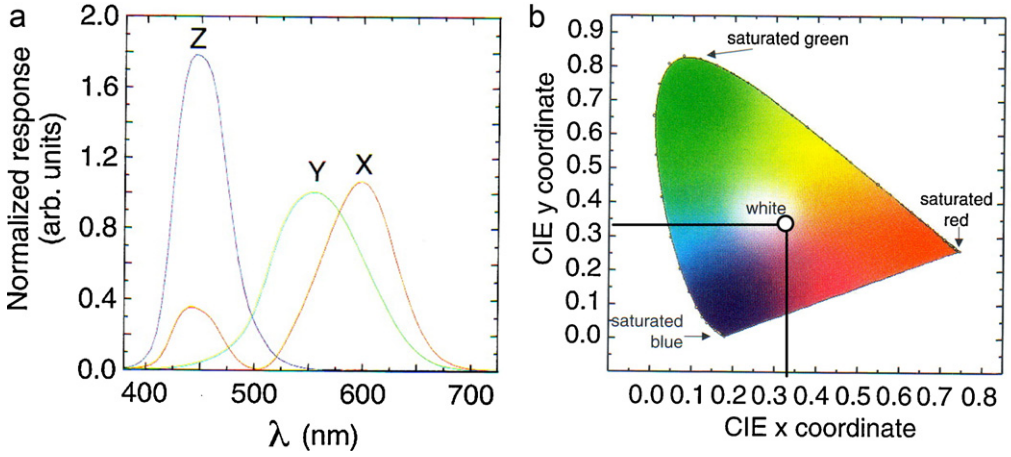

Fig. 3. (a) The CIE standard observer colour-matching functions corresponding to the three colour-sensitive photoreceptors in the eye. Colour coordinates can be calculated by overlapping each of these responses with the emission spectrum of the OLED. (b) The CIE 1931 colour space chromaticity diagram. The diagram represents all of the chromaticities visible to the average person. This diagram displays the maximally saturated bright colours that can be produced by a computer monitor or television set.

we focus on the 'recombination electroluminescence' (REL), that is, the emission of light by an organic luminescent material resulting from recombination of electric field-injected opposite-sign charge carriers (cf. Fig. 1). Perhaps this is the most common type of EL occurring in organics. The essential difference between recombination processes of free carriers in organic and inorganic solids is that the former are concerned with a superposition of energy levels for neutral excited states and ionized states, whereas the latter depend strongly on the band structure. From a kinetic model assuming excited states to be produced throughout the sample in electron-hole recombination process with arbitrary concentrations of electrons, n_e, and holes, n_h, the photon flux per unit area emitted from the EL cell of thickness d can be expressed as

$$\Phi_{EL} = \varphi P_{S,T} \gamma n_e n_h d \quad (7)$$

Here $\varphi = k_r/k_{tot}$ is the emission quantum yield defined by the ratio of the radiative, k_r, to the total, $k_{tot} = k_r + k_n$, decay rate constants for an excited state, including the non-radiative decays with the overall rate constant k_n. $P_{S,T}$ is the probability that in a recombination event a singlet (P_S) or triplet (P_T) excited state will be created. In trap-free materials $P_S = 1/4$ and $P_T = 3/4$ because, due to spin statistics, three times more triplet than singlet excited states are created in the electron-hole recombination characterized by the second order rate constant γ.

In general, only a part of the injected carriers undergoes recombination in organic layers including bulk emitter, the remainder is discharged at the counter electrical contacts, forming the leakage currents. Obviously, the proportion between the recombination and leakage currents determines the light output from EL devices. Studying the kinetics of injected free carriers, this proportion can be translated into the recombination probability $P_R = (1 + \tau_r/\tau_t)^{-1}$ (3), where τ_r is the carrier recombination time and τ_t is the time required for a carrier to traverse the inter-electrode distance d (see Fig. 2). Two limiting cases of the recombination EL have been distinguished based on the value of the recombination-to-transit time ratio: (i) volume-controlled EL (VCEL) for $\tau_r < \tau_t$, that is $P_R > 0.5$, and (ii) injection-controlled EL (ICEL) for $\tau_r > \tau_t$, that is $P_R < 0.5$ [7,8]. The recombination probability $P_R = 0.5$ stands for a demarcation value when the rate of monomolecular decay (leakage current) and the rate of bimolecular decay (recombination current) of the carriers are equal to each other. High recombination EL efficiency requires the τ_r-to-τ_t ratio to be kept at a minimum, then $P_R \to 1$. To exploit this principle for optimizing OLEDs, one needs to understand the processes that control this ratio: (i) the injection of charge carriers, (ii) their transport, and (iii) recombination. Furthermore, the overall quantum EL efficiency as well as spectral features of the emitted light depend on the type and decay pathways of the excited states [8].

2.4. The nature of emissive states

The excited states of molecular solids are traceable to properties of individual molecules. However, their interaction in the condensed phase imposes their collective response called an exciton. If for some reasons, as, for example, energy or charge exchange, a nearby molecule becomes involved to form an excited state, a bimolecular excited state is created. As a consequence, new features in the emission spectrum occur or non-radiative decay of excitons is imposed, reducing the luminescence yield of the system. Various excited states produced by the electron-hole recombination in organic materials are depicted in Scheme II of Fig. 4. Free electrons (e) and holes (h) introduced at suitable electrodes approach each other being able to form either excimer or molecular emissive states. They, by definition, have to pass an intermediate stage of coulombically correlated electron-hole pairs (e. . .h). Due to spin statistics three times more triplet ^{3}(e. . .h) than singlet ^{1}(e. . .h) pairs are created; that is, their creation probability amounts to $P_T = 3/4$ and $P_S = 1/4$, respectively.

Another important point is the structure quality of the luminescent material. In a perfect structure, the LUMOs (lowest unoccupied molecular orbitals) and HOMOs (highest occupied molecular orbitals) of all molecules are on the same level, the charge motion is due to hopping over a barrier dependent only on the molecular structure and intermolecular distance. Radiative electron-hole "cross transitions" between neighbour molecules are highly ineffective in competition with charge recombination on one molecule (indicated by bold crosses in the left-hand side of Fig. 4). Thus, the emission originates from molecular excitons (electrofluorescence or electrophosphorescence) and possibly from singlet and triplet excimers. In disordered structures with defects, the hopping time becomes much longer because an additional barrier (ΔE) for charge hopping can appear due to local defects. Radiative "cross transition" may then become detectable in the long-wavelength wing of the emission. Such "prepared" emissive electron-hole pairs have been named *electromers* [17]. They can be observed in simple molecules of anthracene [18] and more complex molecules [19,20]. Examples of well-resolved electromer emission are shown in Fig. 5. It is noteworthy that, contrary to the two-layer OLED structure of ITO/BTPD-PFCB/P3F1B/Ca, where the electromer emission appears to form the weakest emission band in the red, the electromer emis-

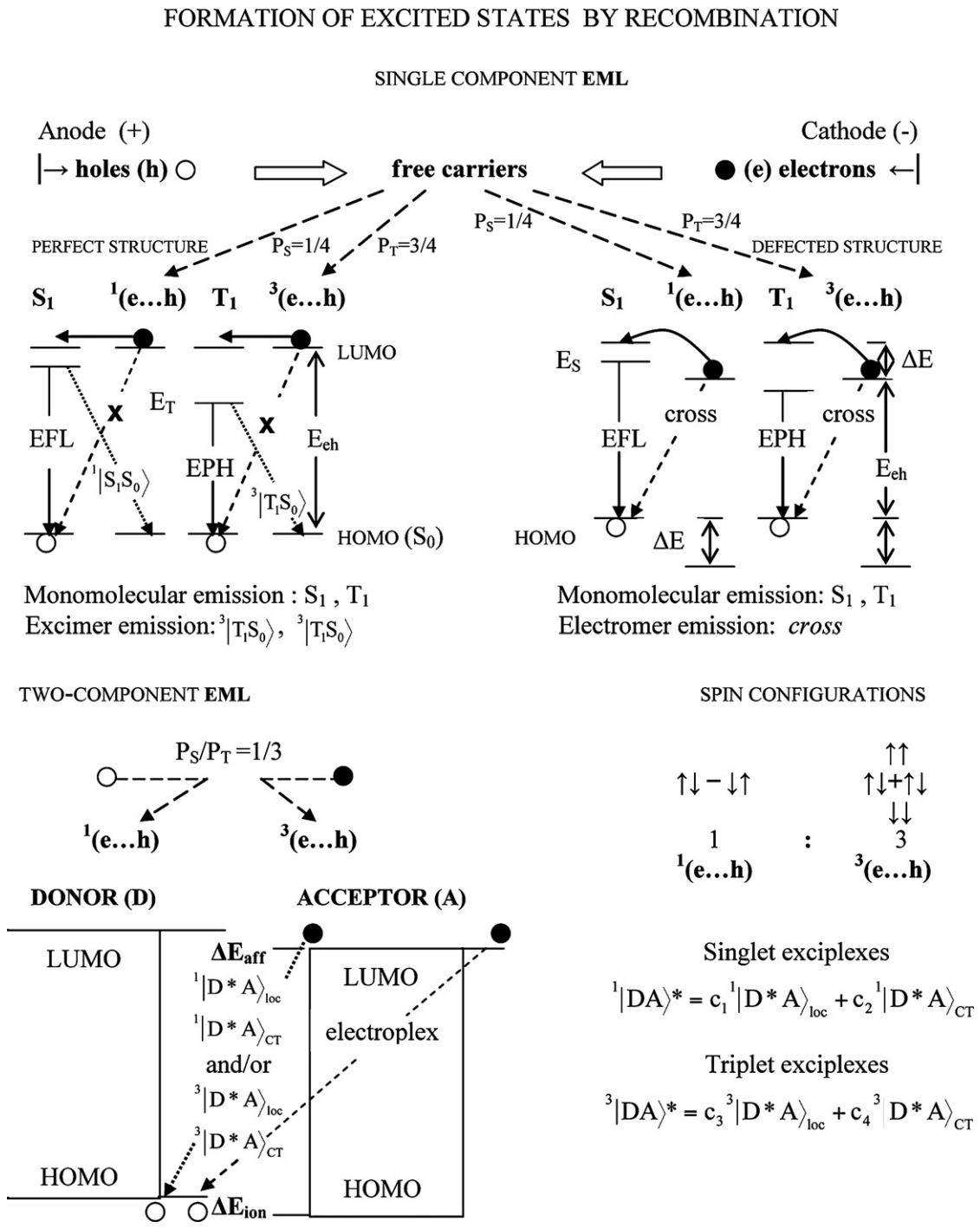

Fig. 4. Various excited states created in the e–h recombination process depicted in an energetic frame of monomolecular and bimolecular states for single- and two-component (electron donor = D and electron acceptor = A molecules) EMLs. The scheme is an extended version of Scheme I (Fig. 2) pointing out the formation of excited states from the injected free charge carriers through intermediates of the coulombically correlated e–h pairs either in their singlet ^{1}(e. . .h) or triplet ^{3}(e. . .h) spin configuration. The emission from vibrationally relaxed monomolecular excited states, S_1 and T_1, is observed as electrofluorescence (EFL) and electrophosphorescence (EPH), respectively. Reprinted with permission from [9]. ©(2008) Elsevier B.V.

sion of the TAPC film forms a dominating red-light band with only traces of the excimer emission in the green emission region.

In two-component blends composed of an electron donor (D) and an electron acceptor (A), the formation of B-M excited states by electron transfer from donor to acceptor molecules is highly facilitated. By analogy to single-component systems, they are called exciplexes and electroplexes (see Fig. 4). An exciplex is a singlet ($^1|DA\rangle^*$) or triplet ($^3|DA\rangle^*$) excited complex of an electron donor and an electron acceptor molecule that is dissociative in the ground state [8] (cf. Scheme II). The dissociative property of the exciplex in the ground state imparts its broad featureless emission band, which is red-shifted from the parent molecules' emission spectra. An example is shown in Fig. 6. The PL and EL spectra of both the electron donor (TPD):electron acceptor (PBD):neutral matrix (PC) system and a double layer (DL) LED (TPD:PC)/PBD differ substantially. The EL spectra are broader and strongly red-shifted with respect to the PL spectra of one-component TPD and PBD-doped films, and exhibit remarkable differences in com-

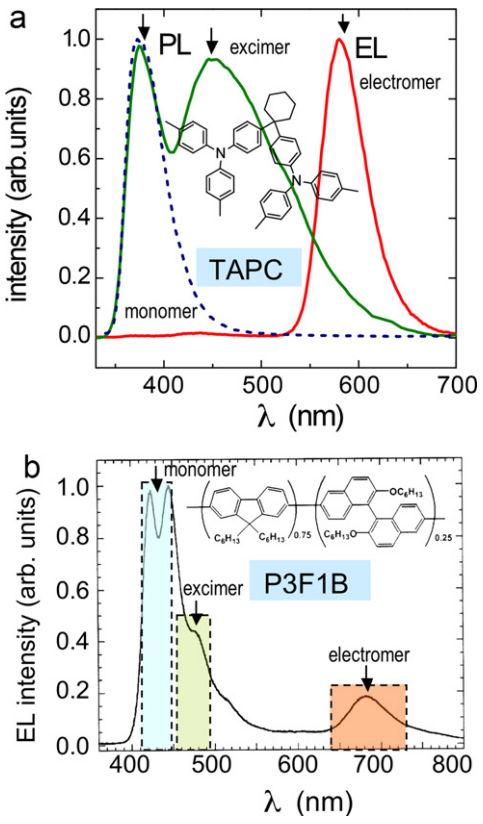

Fig. 5. (a) Comparison of PL and EL spectra of an aryl-amine derivative, TAPC (the molecular structure is given in the background of the figure). The dashed curve is the PL spectrum of TAPC in solution in dichloromethane. Solid lines represent PL (left green) and EL (right red) spectra of a 200 nm-thick vacuum evaporated TAPC film. While the two PL maxima of the film are assigned to the molecular exciton (≈370 nm) and excimer (≈450 nm) emissions, the quasi-unique emission band at ≈580 nm belongs to an electromer. Reprinted with permission from [17]. ©American Institute of Physics. (b) EL spectrum of a two-layer OLED: ITO/BTPD-PFCB/P3F1B/Ca. The molecular structure of P3F1B is given in the inset; BTPD-PFCB stands for a hole-transporting layer composed of bis (*N,N′*-diphenyl-*N,N′*-bis (3-butlphenyl)-(1,1′-biphenyl)-4,4′-amine (BTPD) and a perfluorocyclobutane polymer (PFCB). Apparent EL spectrum features are assigned to different emissive species as indicated in the figure.
Adapted from [19].

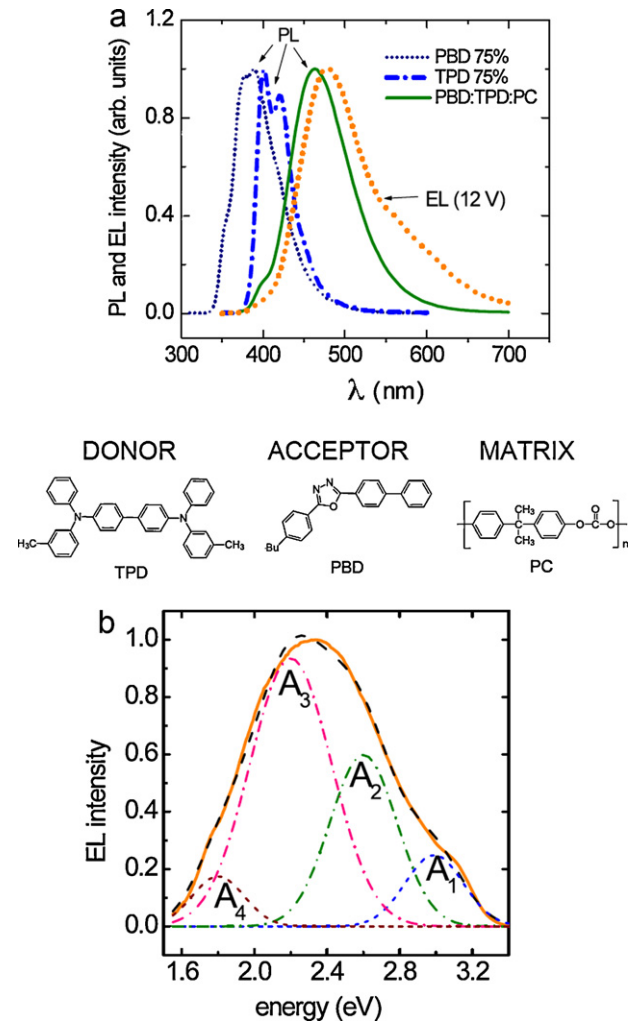

Fig. 6. The PL and EL spectra of a single-layer (a) and the EL spectrum of a double-layer (b). OLED based on an electron donor (TPD: *N,N′*-diphenyl-*N,N′*-bis(3-methylphenyl)-1,1′-biphenyl-4,4′ diamine) and an electron acceptor (PBD: 2-(4-biphenyl)-5-(4-*tert*-butylphenyl)-1,3,4-oxadiazole). The PL spectra of 75 wt% PBD and 75 wt% TPD films in a polycarbonate (PC) matrix are shown in part (a) of the figure for comparison. The EL spectrum of the double-layer LED (b) is deconvoluted into a series of Gaussian bands corresponding to different emissive species as described in the text. Their combination (dashed line) reproduces well the experimental spectrum represented by the solid line. The molecular structures of the materials used are shown in the figure.
Reprinted with permission from [10]. ©Elsevier.

parison with the PL spectra of (TPD:PBD:PC) blend: the DL LED EL spectrum shows much stronger broadening and much larger red shift. The latter has been deconvoluted into four bands showing emission from TPD singlets A_1 ($^1D^* \rightarrow 415$ nm), singlet exciplexes A_2 ($^1|TPD:PBD\rangle^* \rightarrow 477$ nm), and two electroplexes A_3 ($(TPD^+PBD^-)_3 \rightarrow 564$ nm), and A_4 ($TPD^+PBD^-)_4 \rightarrow 670$ nm). Only A_2 and A_3 species are observed in the EL with a single blend emitter (Fig. 6a), the EL spectrum being dominated by the exciplex component A_2. In contrast, the EL spectrum of the DL LED is dominated by the A_3 electroplex band, showing an additional feature A_4 attributed to a trapped electroplex species (Fig. 6b). These observations have been rationalized by different environmental conditions of the e–h recombination processes in the blend layer bulk and on the (TPD:PC)/PBD interface, the latter being rich in a variety of chemical and structural defects favouring the formation of trapped states.

2.5. Recombination and emission zones

The location and width of the e–h recombination regions within the EL structure are of crucial importance for OLED performance. The recombination zone width may be defined as the distance travelled by charge carriers within the recombination time [7]:

$$w_{e-h} = \upsilon_{e,h}\tau_r^{e,h} \quad (8)$$

In general, w_{e-h} for electrons and for holes is different because of a difference between their velocities, $\upsilon_e \neq \upsilon_h$, and recombination times, $\tau_r^e \neq \tau_r^h$. It should be noted that such defined recombination zone width must not be identified with the geometrical limits imposed on the charge recombination by the device structure. For EL study, when the light emission is of interest, the upper limit of w_{e-h} becomes more relevant. Whether, and eventually, how the recombination zone changes with the applied electric field (F) depends on the velocity with which the carriers move and on the character of the current flowing through the sample. At low electric fields, when the thermal velocity exceeds the drift velocity,

$v_{e,h} \cong v_{th}(F) = \text{const}$, and for comparable contribution to the current of holes and electrons ($\mu_h n_h \cong \mu_e n_e$) we arrive at

$$w_{e-h} = \left[\frac{2\mu_{e,h}\varepsilon_o\varepsilon v_{th}}{e(\mu_e + \mu_h)}\right]\left(\frac{F}{j}\right) \quad (9)$$

using the Langevin's expression for γ:

$$\gamma \cong \frac{e(\mu_e + \mu_h)}{\varepsilon_o\varepsilon} \quad (10)$$

From Eq. (9) it follows that whenever j is a superlinear function of F, w_{e-h} becomes a decreasing function of the applied electric field. The functional shape of the field-dependent w_{e-h} results from the current–voltage behaviour of the EL cell. The recombination zone contracts as F^{-1} for ohmic carrier injection,

$$j = \frac{9}{8}\varepsilon_o\varepsilon\mu_{eff}\frac{F^2}{d} \quad (11)$$

and becomes approximately an exponential function of the form $\exp(-\beta F^{1/2})$, for the currents limited by the field-assisted thermionic injection [7].

The recombination zone at high fields, since the carrier velocity approaches the drift velocity, is determined by the recombination-to-transit time ratio:

$$w_{e-h} = \left(\frac{\tau_r^{e,h}}{\tau_t^{e,h}}\right) d \quad (12)$$

Thus, a simple relation between the recombination width and recombination probability can be obtained by combining Eq. (12) with (3)

$$P_R = \frac{1}{1 + (w_{e-h}/d)} \quad (13)$$

The two limiting operation modes of the EL cell lead then to important consequences for $w_{e-h} : w_{e-h} > d$ for the ICEL and $w_{e-h} < d$ for the VCEL operation mode (cf. Section 2.3). When we apply Langevin's theory of recombination (10), substituting at the same time definition relations for τ_r and τ_t (8) for comparable contribution to the current of holes and electrons, we obtain

$$w_{e-h} \cong \left[\frac{2\varepsilon_o\varepsilon\mu_e\mu_h}{\mu_e + \mu_h}\right]\left(\frac{F^2}{j}\right) \quad (14)$$

Accordingly, the recombination zone varies with electric field in a manner slightly different from that in the case of diffusion motion of charge carriers (see Eq. (9). But, for strongly field dependent ILC, $w_{e-h} \propto j^{-1}$ in both cases. However, in contrast to Eq. (9), Eq. (14) predicts a field-independent w_{e-h} for the superlinear function of $j(F)$ if ohmic injection occurs at the contacts. The applied field produces then a current given by Eq. (11) and

$$w_{e-h} \cong \frac{2\mu_e\mu_h d}{(\mu_e + \mu_h)\mu_{eff}} \quad (15)$$

which, in the case of negligible space-charge overlap ($\mu_{eff} \cong \mu_e + \mu_h$), gives within a factor of 2, the width of the recombination zone derived from an analysis of the recombination-induced coordinate variation of charge carrier concentration [21,22].

In addition to the recombination zone, the term of EL emission zone is used when characterizing the EL light source. The recombination and EL emission zones are sometimes identified with each other but a closer look at them shows that they should differ because of the mobility of excited emissive states, reabsorption and light guide effects. On this basis, the EL emission zone is expected to exceed the recombination zone, though an opposite relation can occur in EL devices with non-homogeneous distribution of exciton and charge traps and those containing non-emissive layers. In a trap-free emitter with two ohmic electrodes, the location of the single luminous layer (EL emission zone) is determined by the ratio of electron and hole mobilities and its width by the relation between these mobilities and the so-called recombination mobility, $\mu_0 = \varepsilon_0\varepsilon\gamma/2e$ [22,23]. For example, the EL emission zone in the c' crystallographic direction of a trap-free tetracene crystal is calculated to be located at $0.23d$ from the cathode and have width of $0.4d$, but traps affecting drift and recombination mobilities along with triplet exciton quenching on trapped charge carriers change this picture entirely as exemplified in Fig. 7. The EL emission is stratified, showing maxima in the vicinity of both electrodes as reported in the unique works by Kalinowski and coworkers (cf. Refs. [7,8,23]). It is interpreted as a strong e–h recombination near the electrodes where the charge has been accumulated filling there the heavily populated traps: a high concentration of singlet excitons is generated and strong prompt EL (PEL) follows from these regions. At high voltages, a third though weak emitting region appears following the principal anode lighting. This region has been ascribed to the delayed EL (DEL) emitted by singlet excitons generated in the exciton triplet–triplet fusion (see Section 2.4). The DEL becomes largely reduced towards the anode because the triplets become efficiently quenched by exponentially distributed concentration of trapped holes. As a result, a minimum in the overall EL intensity occurs at ~17 μm, and the EL lighting shows up as divided into three subzones. In general, the emission pattern depends critically on injection ability of the electrodes and charge distribution gradients (hence on the concentration and distribution of traps, in turn dependent on the crystal quality). For example, no third emission region can be observed at lower voltages in the EL intensity pattern as shown in Fig. 7 for tetracene, and no cathode lighting zone has been reported in anthracene crystals [23]. It is clear from Eq. (13) that to maximize the OLED efficiency requires the minimizing of the recombination zone ($P_R \to 1$ for $w_{e-h} \to 0$). The efforts focus on the confinement of the recombination process to a thin emissive layer. Various ways are used to reach this goal, from varying dopant concentration in the EML along with optimized driving voltage [24,25] to introducing into the OLED architecture charge carrier and mobility blocking layers [26–28].

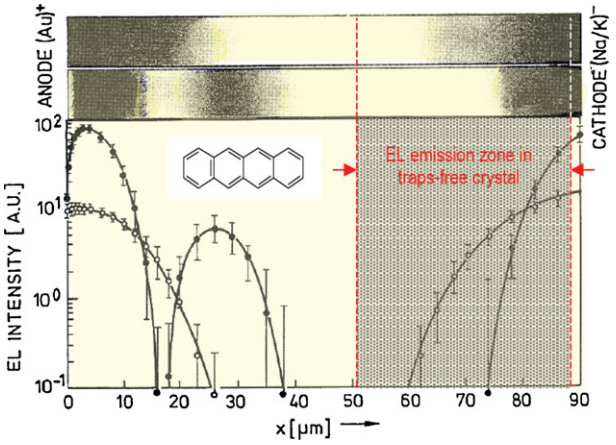

Fig. 7. Spatial distribution of EL intensity in a 90 μm-thick tetracene crystal at two different voltages: $U = 750$ V (open circles), $U = 950$ V (filled circles). The semi-transparent hole-injecting Au anode is arbitrarily located at $x = 0$, and a thick layer of the Na/K alloy forms an electron-injecting contact at $x = 90$ μm, where x is the axis directed perpendicular to the crystallographic (ab) plane of tetracene. The dark field patterns in the upper part simulate the light intensity distribution for these two voltages (lightly yellow background represents spurious scattered light). The EL emission zone as predicted for tetracene crystal for volume-controlled currents with small space-charge overlap is indicated by the vertical dashed lines for comparison. Adapted from [23].

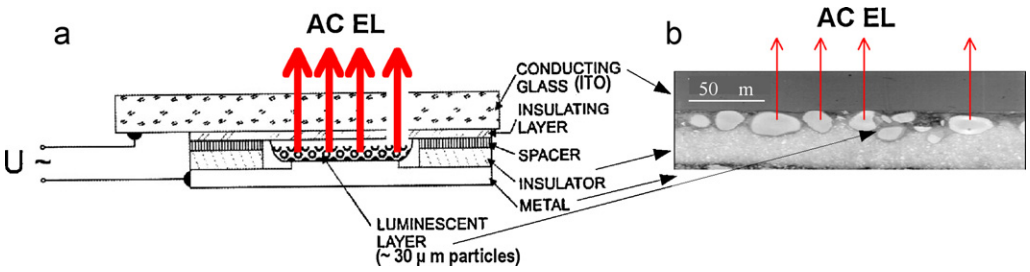

Fig. 8. Schematic view (a) and magnified real (b) cross section of ACTFEL (alternating current thin film electroluminescence) devices. An alternating-current voltage ($U\sim$) is necessary for continuous electroluminescent emission from microcrystals suspended in an insulating medium, the effect being observed with inorganic phosphors or from luminescent materials containing electron-injecting particles.
Adapted from [7] (a) and from the Oregon University NanoLab/NSF photograph placed in the authorSTREAM.com (b).

2.6. Classification of OLEDs

There are various criteria to classify OLEDs. They are based mostly on the nature of the emitting states involved in the EL emission, but the emission colour or serving purpose are often invoked for classifying the OLEDs. Accordingly, the OLEDs emanating from singlet molecular excitonic states can be named fluorescent OLEDs (FOLEDs), a typical example of which is an OLED based on Alq_3 as the emitter [29]. Such named OLEDs must not be confused with "FOLEDs" ascribed to OLEDs built on flexible (F) substrates [30], thus another acronym, FLOREDs, could perhaps be more suitable. OLEDs revealing emission from excited triplet molecular states have been named phosphorescent OLEDs (PHOLEDs). There are numerous examples of PHOLEDs based on various phosphorescent materials. All heavy atom-substituted organic molecules are predisposed to form EMLs for PHOLEDs. An archetypal material is a platinum porphine: PtOEP = 2,3,7,8,12,13,17,18-octaethyl-21*H*,23*H*-porphine platinum (II) [31]. Clearly, all organic iridium and platinum complexes will fall in this category of OLEDs when emitting from monomolecular triplet states. If the emissive species are triplet B-M excited states, i.e. triplet excimers or triplet exciplexes, then the OLEDs, though still preserving phosphorescent operating mode, are called excimer or exciplex OLEDs (EXLEDs). Obviously, OLEDs emitting from singlet excimers or exciplexes also belong to the EXLED category, but they are not PHOLEDs.

The distinctive feature of OLEDs is that they are able to produce various emission colours in accordance with a wide selection of organic compounds. Much of the research has focused on light emission in the visible range. However, there are numerous applications (optical communication and biomedical among the most prevalent) calling for optoelectronic devices operating in the saturated red and near infrared (NIR) spectral regime. The extension of efficient OLEDs into the technologically important near-infrared (NIR) spectral range (NIROLEDs) is challenge to scientists and engineers. Various approaches have been explored to obtain infrared emission from organic LEDs. The use of rare earth complexes and small optical-gap polymers has been attracting interest, since lanthanide ions such as Er^{3+} or Nd^{3+} emit in the NIR, and polymer emission can extend to a wavelength of 1000 nm. One of the most important shortcomings of current NIROLEDs is poor quantum efficiency and low power output. For example, forward light output of 100 $\mu W/cm^2$ and only 0.1% of external quantum efficiency have recently been reported for NIR electrophosphorescence with a peak value at 720 nm from blends of polymeric host and an iridium (III) complex [32]. A dispersion of inorganic indium arsenide-based nanocrystals in conjugated polymers has been employed to improve the quantum efficiency, but to no more than ≈0.5% ph/e [33]. Only recently, the application of generating excimer phosphorescence of neat films made of terdentate Pt(II) complexes has enabled the fabrication of highly efficient (up 10% ph/e) NIROLEDs, as reported earlier by our group (see Section 5.1).

White-light emitting OLEDs (WOLEDs) can be fabricated on the basis of both fluorescent and phosphorescent organic materials. Ideal white light CIE coordinates are ($x = 0.33$, $y = 0.33$); those for warm incandescent lamp light are (0.41, 0.41) with CRI = 100 (see Section 2.2). Phosphorescent WOLEDs generally are more efficient (maximum power efficiency ~ 42 lm/W [34]) as compared to 6 lm/W for small-molecular [35] and polymeric [36] fluorescent WOLEDs. With an improved architecture, using a periodic outcoupling structure, a device power efficiency 90 lm/W at 1000 cd/m^2 has been achieved for a WOLED based on an EML combined of different organic phosphors [37]. A particular type of OLEDs for plant growth, PGOLEDs, has recently been put forward [38]. They are light sources with a rather specific emission profile that corresponds to the action spectrum of photosynthesis, and thus can be used to optimize the efficiency of plant growth by providing the most appopriate wavelengths of light in the correct proportions. They will enable researchers and agriculturists to eliminate those wavelengths within normal white light that are largely inactive in photosynthesis, thus reducing the amount of energy to power plant growth lamps (see Section 7).

In this context, alternating-current thin-film-electroluminescent (ACTFEL) devices should be mentioned as they can realize an innovative lighting technique and informative display panels. ACTFEL devices are essentially just capacitors with a powder-type luminescent layer as shown in Fig. 8. The common feature of the powder-type EL cells is the creation of high local electric fields enabling charge injection at the interface of conducting, luminescent material particles. Light emission appears as a result of impact ionization and excitation by injected carriers accelerated in the strong interfacial electric field (the impact EL mechanism) [7,16]. Since our focus is on the recombination-type of EL, and since ACTFEL devices are rarely based on organic materials, their further discussion is beyond the scope of this review.

Finally, we mention the transparent OLEDs (TOLEDs) category. They use a transparent contact to create displays that can be made to be top-only emitting, bottom-only emitting, or both top- and bottom-emitting (transparent) (cf. Section 2.1). Copper phthalocyanine (CuPc) capped with a film of low-power radio frequency sputtered indium tin oxide has been reported as a metal-free transparent cathode for an OLED based on the archetypal emitter Alq_3 [39]. More recently, devices that are transparent throughout the visible spectrum have been prepared using indium gallium zinc oxide as the upper electrode [40]. TOLEDs can greatly improve contrast, making it much easier to view displays in bright sunlight. Because TOLEDs are 70% transparent when turned off, they

may be integrated into car windshields, architectural windows, and eyewear.

3. Light emitting materials. Why cyclometallated Pt complexes?

Of the various heavy metal ions that could be envisaged for promoting radiative emission of triplet states in OLEDs, iridium(III) and platinum(II) have attracted the most attention to date. Not only do they have high spin-orbit coupling constants, but they can form discrete, kinetically inert, charge-neutral coordination complexes with aromatic ligands. Flourishing studies over the past decade have revealed how the excited state energies and hence colour in several classes of their complexes can be controlled through rational ligand design [41–45]. Calculations using, for example, density functional theory (DFT) and time-dependent DFT (TD-DFT) have proved particularly useful in this respect: in many cases, the magnitude of the HOMO-LUMO gap provides a qualitative guide to the emission energy. Some level of prediction of the extent to which the formally forbidden triplet radiative processes become allowed may also be provided by such calculations, for example, by considering the extent to which the metal atomic orbitals participate in the frontier orbitals involved in the lowest-energy excited states [44]. Meanwhile, simple concepts such as the rigidity of the complex and assessment of ligand-field strengths can help to provide a qualitative indication of the extent to which non-radiative decay may limit the performance [42]. As noted earlier, the emission quantum yield for an isolated complex is determined by the relative magnitudes of the rate constants of radiative and non-radiative decay, $\varphi = k_r/(k_r + k_{nr})$, and so a qualitative appreciation of the molecular properties influencing these parameters is crucial in the design of highly emissive phosphors.

We previously reviewed these concepts for platinum [6,42,46], and the reader is directed to those reviews for a more detailed discussion. In this section, we provide a brief summary of the key points and highlight some of the molecular structures that offer the highest efficiencies, before considering their application in OLEDs in the subsequent sections.

Of the three generalised classes of excited states encountered in d-block complexes (metal-centred d–d states; ligand-centred states – usually π–π^*; charge-transfer states – usually MLCT), the d–d states are rarely emissive, owing to distortion of the molecule in the excited state. For platinum(II), the formation of the d–d state involves the population of the highly antibonding d_{x2-y2} orbital, such that the Pt–L bond lengths will increase in the excited state. Distortion favours non-radiative decay. A key to minimising non-radiative decay is thus to ensure that d–d states are not energetically accessible at room temperature: successful complexes will have lowest-lying CT or LC states, and the energy gap to the higher lying d–d states will be substantially greater than kT [47]. This leads to the requirement for strong field ligands, to ensure a large gap between the filled d_{xy} and vacant d_{x2-y2} metal orbitals. Meanwhile, the use of rigid, chelating ligands should help to minimise non-radiative decay.

From both points of view, aromatic cyclometallating ligands are attractive. The archetypal ligand of this type is 2-phenylpyridine (ppyH), which can bind to metal ions like Pt(II) through the pyridine nitrogen atom and the deprotonated carbon atom adjacent to the interannular bond (coordination mode denoted N$\hat{C}$, e.g. as in Fig. 9a). The combination of the strong σ-donating carbon atom of the metallated phenyl ring and the π-accepting pyridyl ring leads to a strong ligand field, while the 5-membered chelate ring generated imposes a desired element of rigidity on the complex. Despite these attractive features, however, the identity of the remaining ligands also proves crucial in determining whether Pt(N$\hat{C}$-ppy) complexes are emissive. For example, $[Pt(ppy)Cl_2]^-$ is not luminescent at room temperature [49], whereas Pt(ppy)(acac) is (Fig. 9a) [48,49].

Pioneering work by Thompson et al. revealed how modification of the aryl or pyridyl rings can allow tuning of the excited state energy in Pt(N$\hat{C}$) complexes [49]. To a first approximation, the aryl group predominantly influences the HOMO energy while the pyridyl (or other heterocycle) is more important in determining the LUMO energy. Electron donors destabilise orbitals (be they HOMO or LUMO), and electron acceptors stabilise orbitals. A remarkable degree of control over the colour of emission can be achieved using this simple concept, although the quantum yields tend to fall off for high-energy (blue) emitters, probably since the energy gap to the higher lying d–d state necessarily becomes smaller.

A number of researchers have since made use of Pt(II) complexes incorporating N$\hat{C}$-bound ligands based on phenylpyridine [50–55]. Liquid crystalline systems have been reported recently, which carry long alkyl chains appended along the same axis as the interannular C–C bond, e.g. Fig. 9b [56]. Interestingly, these compounds also have the highest photoluminescence quantum yields hitherto reported for Pt–ppy complexes. This high performance ($\varphi_{lum} > 0.5$) seems to be associated not with the presence of the long chains, but rather with the substitution pattern: an alkoxy substituent at position 5 of the phenyl ring and alkoxyphenyl at position 5 of the pyridyl ring, where n (Fig. 9b) can be as small as 1. This substitution seems to reduce not only the non-radiative decay constants, but also the radiative decay rate, leading to unusually long luminescence lifetimes ($\tau = 27\ \mu s$). Though a little too long to be ideal as OLED phosphors, the study demonstrates how very efficient emitters can be generated from relatively unsophisticated ligand systems. Another recent innovation has included the covalent attachment of moieties designed to facilitate charge transport, pioneered in particular by Wong and co-workers [57]. These units have included main group elements such as boron, germanium and silicon (e.g. Fig. 9c), and improved hole and/or electron injection is reported. Complexes based on the Pt(N$\hat{C}$)(acac) structure incorporating the hole-carrier unit triphenylamine have also been studied [58].

The Pt(N$\hat{C}$)(acac) unit has recently been incorporated covalently into a polymer by ring-opening metathesis copolymerisation of norbornene-appended complexes with a norbornene-appended carbazole (Fig. 9d) [59]. This approach may offer a solution to problems with phase separation sometimes encountered in blends of small-molecule phosphors and polymers. Both the PL and EL spectra of films formed from the polymer display a combination of monomeric and excimer/aggregate emission.

An exciting new development in the design of Pt(N$\hat{C}$)-based complexes is emerging from the work of Weck and co-workers [60] and, independently, Huo and co-workers [61]. They have been investigating tetradentate ligands, in which two N$\hat{C}$-coordinating ppy units are attached to one another through a single atom linker, either a carbon atom *ortho* to the coordinated pyridyl nitrogen atoms in the first case (Fig. 9e and f), or a nitrogen atom *ortho* to the metallated carbon atoms (Fig. 9g). The extra rigidity associated with the tetradentate structures may be anticipated to disfavour non-radiative decay and, indeed, quantum yields in excess of 0.5 have been recorded for several of these structures at room temperature, considerably superior to the conventional bis-bidentate complexes.

Another way of increasing rigidity is to make use of terdentate ligands. Square-planar complexes comprised of two bidentate ligands, M(L$\hat{L}$)$_2$, are unstable with respect to a D_{2d} distortion, namely a twisting of the plane of one ligand relative to that of the other, away from square planar and towards a tetrahedral conformation [62]. Such distortion facilitates non-radiative decay by promoting coupling with the ground state. Ligands based on three

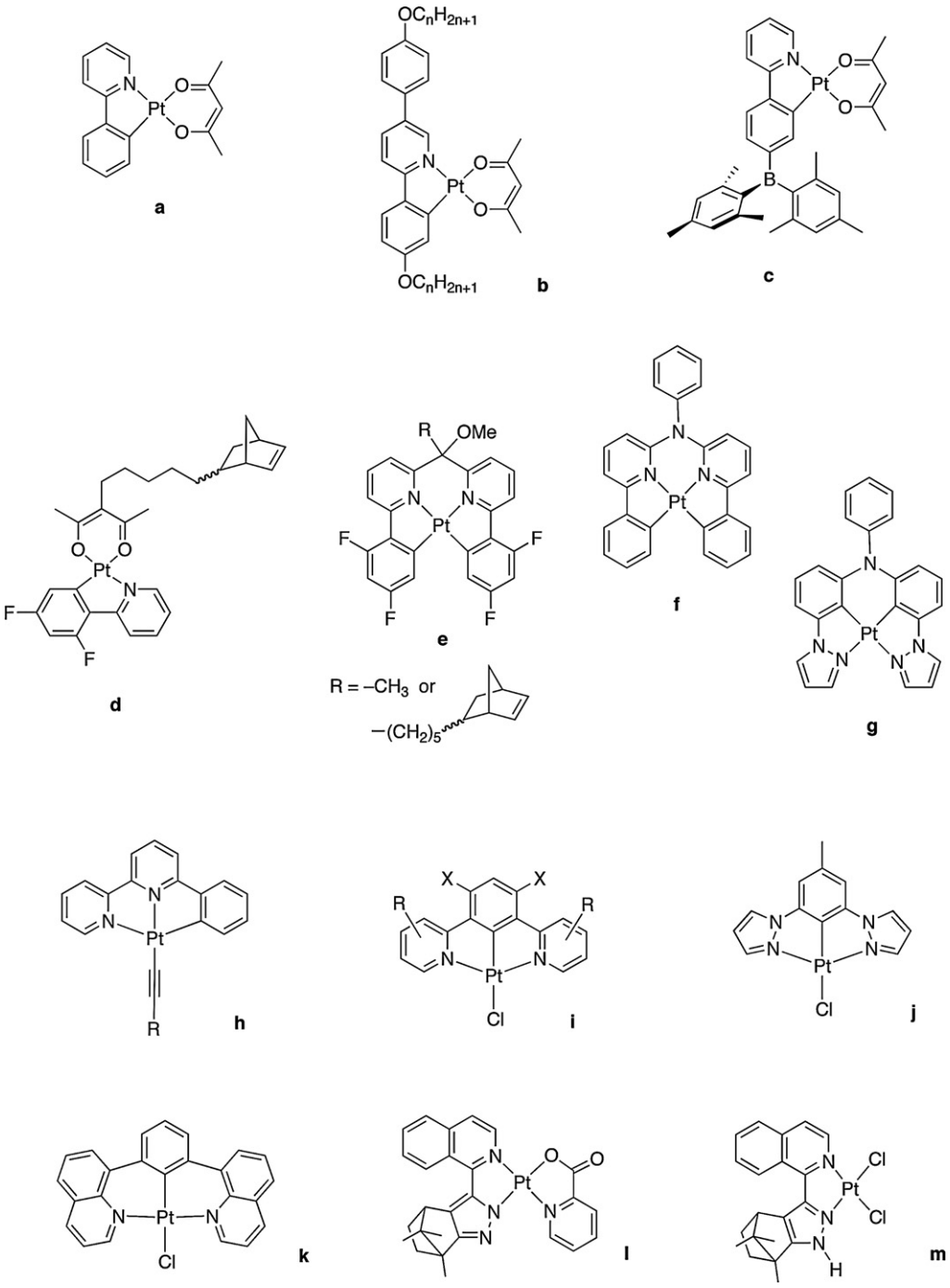

Fig. 9. Structures of some of the cyclometallated platinum complexes (**a**–**k**) discussed in the text. Also shown are structure **l**, a pseudo-metallate comprising a deprotonated azole nitrogen analogous to a metallated carbon atom, and its precursor **m**.

aromatic rings linked through *meta*-related positions of the central ring, and of which terpyridine is the archetypal example, should offer greater rigidity, inhibiting such distortions. Cyclometallating terdentate ligands which offer the metal ion NN̂C, NĈN, or CN̂C coordination have all been explored with platinum(II), based on 6-phenylbipyridine, 1,3-dipyridylbenzene and 2,6-diphenylpyridine respectively [63–65].

Most relevant to OLEDs are the first two classes, which are monanionic ligands. Pt(NN̂C)X complexes can be quite strongly emissive, particularly when the fourth, monodentate ligand X provides a strong ligand field, such as acetylides, –C≡C–R (Fig. 9 h). Che and co-workers reported a comprehensive study of the synthesis and photophysics of such complexes including their application in OLEDs [66].

Meanwhile, many Pt(NĈN̂)X complexes (e.g. X = Cl, Fig. 9i) display exceptionally high luminescence quantum yields, up to 0.85 in solution at room temperature [64]. Colour tuning across the visible spectrum can be achieved through rational ligand modification (opposing effects of substituents in pyridyl and phenyl rings), in a similar way to that described earlier for the Pt(ppy)(LX) complexes [67]. The terdentate ligands prove to be superior, however, in that the high quantum yields of their complexes are retained even for bluer emitters. A theoretical analysis of the three classes of cyclometallating terdentate ligands suggests that the superi-

ority of the Pt(NĈN̂) systems is associated with a high degree of rigidity, with little geometrical reorganisation in the excited state compared to the ground state [68]. Experimental testament to this conclusion is provided from variable-temperature luminescence measurements down to 1.2 K [69]. A number of the OLED systems described in the sections that follow make use of this class of complex.

The use of other heterocycles such as pyrazoles in place of the pyridyl rings has also been investigated (Fig. 9j) [70]. While the poorer π-acceptor nature of pyrazole compared to pyridine predictably leads to an increase in the excited state energy and thus to a shift to the blue, the bite angle offered by the ligand seems to be less suited to binding the platinum ion, and the quantum yields are inferior, probably due to facile non-radiative decay associated with distortion. Another development with different heterocycles involves the use of quinoline-based ligands, linked to the central ring via their 8-position. Unusually, these ligands form 6-membered chelate rings when they bind to platinum(II) (Fig. 9k); most ligands bind through 5-membered rings. The larger ring size should relieve strain associated with the sub-optimal bite angle of ligands such as 1,3-dipyridylbenzene, and indeed a crystal structure reveals the NĈN̂ angle to be approx 180° in the former compared to around 160° in the latter. Although this might be expected to disfavour non-radiative decay {as is observed for the corresponding NN̂N̂N-coordinated 2,6-di(8-quinolinyl)pyridine complex compared to [Pt(tpy)Cl]$^+$}, the emission efficiency of the new complex is actually rather inferior to comparable complexes of dipyridylbenzenes, apparently due to a smaller radiative rate constant [71].

Finally, we note that NN̂$^-$ ligands can be regarded as "pseudo-cyclometallating" ligands and can also lead to highly luminescent platinum(II) complexes. Here, N$^-$ represents a deprotonated azole nitrogen, as in a pyrazole, indazole, imidazole or triazole, and N represents a neutral nitrogen donor such as a pyridine or quinoline ring. The N$^-$ ligation is comparable to the metallated carbon of a cyclometallating ligand like ppy. For example, the complex in Fig. 9l has $\varphi_{lum} = 0.64$, $\tau = 8.2$ μs in solution at room temperature [72]. The importance of the deprotonation of the azolic nitrogen atom to give a strong σ donor and hence augment the ligand field is evident from comparison with the complex in Fig. 9m, an NN̂-coordinated analogue, which is non-emissive under the same conditions.

4. Phosphorescent OLEDs (PHOLEDs)

The emission spectrum and hence the colour of Pt(II) complex-based OLEDs depends on the strength of singlet-triplet mixing in emissive molecules, and on their propensity to form B-M excited states in the EMLs. In general, phosphorescence occurs from a mixture of LC and MLCT transitions (see Section 3). The relative importance of the MLCT and LC components depends on their energetic separation. For example, the MLCT component of PtOEP phosphorescence is very small because the porphin ligand has a significantly lower triplet energy [73]: the emission is dominated by the LC transition giving relatively narrow PL and EL spectra centred at ≈650 nm [74] (see Fig. 9b). Furthermore, the PtOEP triplet localized on the ligand experiences relatively inefficient spin-orbit mixing with the central Pt atom, and consequently, its lifetime may be as long as 100 μs [74]. This long triplet lifetime increases the problem of triplet quenching in the triplet–triplet and triplet-charge carrier annihilation processes, which leads to a strong roll-off in the EL efficiency at high current densities [75,76] (cf. Sections 2.2 and 5). Long phosphorescence lifetimes can also limit display speeds and refresh rates. Shorter phosphorescent lifetimes are thus desirable, of the order of microseconds rather than hundreds of microseconds.

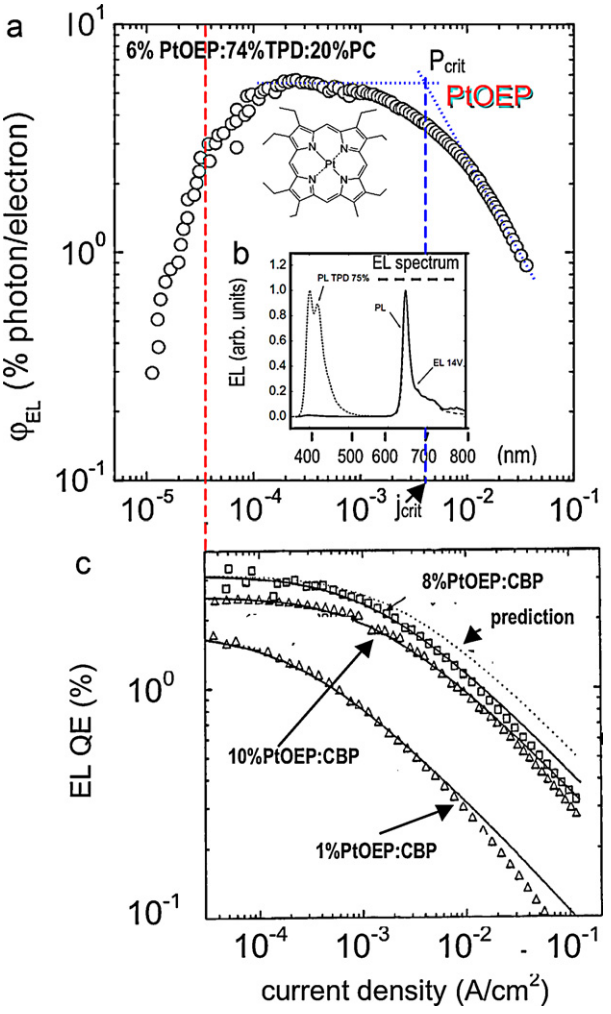

Fig. 10. External quantum efficiency of two PtOEP-doped EML OLEDs evolving with driving current density: (a) ITO/6 wt% PtOEP:74 wt% TPD:20 wt% PC (60 nm)/100% PBD (60 nm)/Ca, where TPD, PBD and PC are described in Fig. 6; the $j = j_{crit}$ sets the point P_{crit} where the T–T annihilation levels off with the monomolecular decay of emissive triplets. (b) the PL and EL spectra of the OLED along with the PL spectrum of TPD. (c) ITO/100% α-NPD(40 nm)/x wt%PtOEP(100 − x)CBP(10 nm)/100%BCP(20 nm)/100%Alq$_3$(20 nm)/MgAg, where α-NPD (4,4′-bis[*N*-(1-napthyl)-N-phenyl-amino]biphenyl) forms the HTL; CBP (4,4′-*N*,*N*′-dicarbazole-biphenyl) is a host material for the PtOEP emissive dopant; the thin layer of bathocuproine (BCP) (2,9-dimethyl-4,7 diphenyl-1,10-phenanthroline) acts to confine excitons within the formation zone centred adjacent to either the Alq$_3$/α-NPD or the CBP/BCP interface; and the Alq$_3$ layer acts as ETL. Figure points represent the experimental data, solid lines in part (c) are the fits according to Eqs. (2) and (3) with an assumption $P_R = P_d = 1$ and $P_q(j)$ approximated by $P_{qi} = (1 + \tau_{0i}/\tau)^{-1}$ with $\tau^{-1} = \tau_{0i}^{-1} + (1/2)\gamma_{TT}T$.
The data are adapted from [74] {(a) and (b)}, and [75] (c).

On the other hand, the emission from cyclometallated Pt complexes, such as those in Fig. 9, is typically attributed to a strongly mixed ^{3}LC-MLCT state [49]. The metal's influence in promoting triplet radiative decay is increased, and the natural radiative lifetimes of many of these compounds are of the order of 10 μs, much shorter than those of platinum porphyrins. At low complex concentration (≤5 wt%) in the so-called doped OLEDs, the formation of B-M excited states is inefficient and practically only the monomolecular (M-M) excited triplet states are generated in such EMLs (cf. Section 2.4). In doped OLEDs, different molecules perform the functions of electron-hole transport and of the emission. Such separation of functionality allows for optimization of device performance.

Fig. 10 illustrates the current density evolution of the external quantum efficiency (EL QE or φ_{EL}) for two PHOLEDs doped with

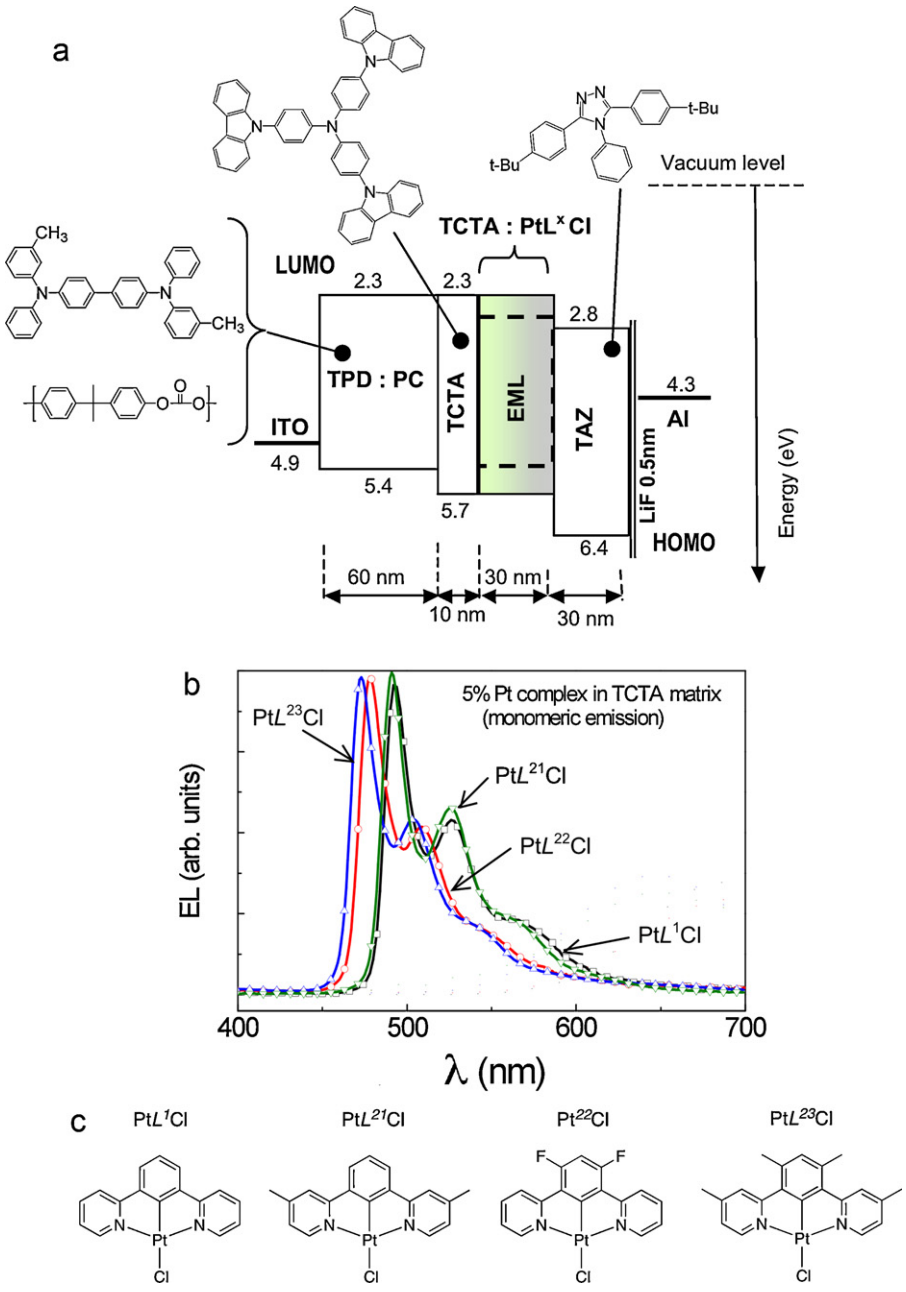

Fig. 11. (a) The architecture of the PHOLEDs based on PtL^nCl complexes as emitters. It is completed with molecular structures of the materials used and energy level diagram shown for understanding the exciton and electronic traffic within the devices. (b) The EL spectra of the PHOLEDs with the 5 wt% PtL^nCl complex-doped TCTA EMLs along with (c) the molecular structures of the complexes used. Each curve is normalized to the intensity integrated over the total spectral range.
Adapted from [77].

varying concentration of PtOEP into their different EML matrices. For PtOEP-doped (TPD:PC) EML (a), the full evolution from the lowest current densities is seen: following an initial increase, the EL QE becomes constant and then a typical roll-off occurs at the largest current densities. The latter two segments are displayed for the PtOEP-doped CBP EML (c) at varying concentration of the dopant (experimental figure points). Solid lines represent fits following Eqs. (2) and (3) with a simplifying assumption $P_R = P_d = 1$, $P_{si} = 3/4$, and

$$\varphi_{EL}^{(ext)}(j) = \left(\frac{3}{4}\right)\xi(j)\varphi^{PL}P_{qi}(j) \cong \left(\frac{3}{4}\right)\xi(j)\varphi^{PL}\frac{\tau}{\tau_0} = \left(\frac{3}{4}\right)\xi(j)\frac{\varphi^{PL}}{\tau_0}\left(\frac{ew_{e-h}}{j\gamma_{TT}}\right)^{1/2} \quad (16)$$

where $\tau^{-1} \cong \gamma_{TT}T$ has been taken for the high triplet exciton concentration region (in Fig. 10, large current densities region above j_{crit}) within which τ decreases as $j^{-1/2}$ and triplet exciton decay is dominated by the triplet–triplet annihilation process with the second order rate constant γ_{TT} [76]. For PHOLED (a) in Fig. 10, assuming the complete recombination confinement to the EML, that is $w_{e-h} \approx d_{EML} = 60$ nm, with $\xi(j) = \text{const} = 0.2$, $\varphi^{PL} = 0.5$ [73] and $\tau_0 = 70$ μs [74,75], Eq. (16) at $j = j_{crit}$ gives $\gamma_{TT} = 9 \times 10^{-14}$ cm^3/s. Similarly, $\gamma_{TT} = (3 \pm 1) \times 10^{-14}$ cm^3/s for the 8% PtOEP:CBP device (Fig. 10c) follows taking into account the monomolecular decay of emissive triplet states $\{\tau^{-1} = \tau_0^{-1} + (1/2)\gamma_{TT}T\}$ and fitting the ratio of the $\varphi_{EL}^{(ext)}(j)$ in the presence and $\varphi_{EL}^{(ext)}(j) = \varphi_0$ in the absence of T–T annihilation, $\varphi_{EL}^{(ext)}(j)/\varphi_0 = (j_0/4j)[(1 + 8j/j_0)^{-1/2} - 1]$ with $j_0 = 4ew_{e-h}/\gamma_{TT}\tau^2$ [75]. It should be noted here that these approxi-

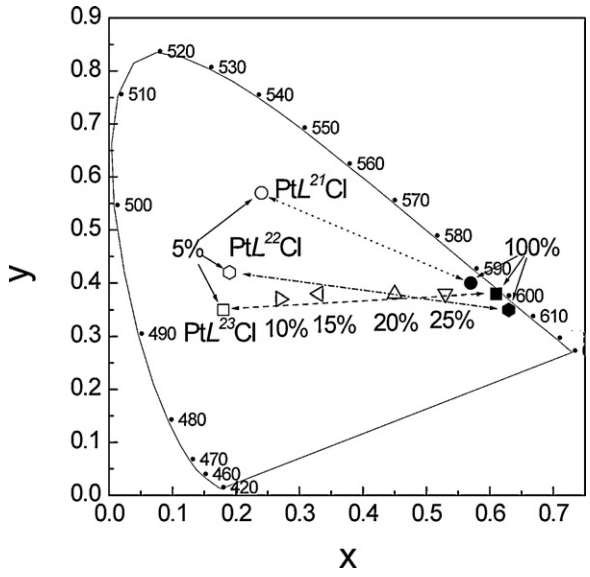

Fig. 12. CIE coordinates (x, y) [as defined in Eq. (6)] of selected PtL^nCl-doped PHOLEDs. The coordinate change with complex substituents and concentration of the dopant for the most efficient PHOLED (PtL^{23}Cl) illustrate the high ability to diversify the PHOLED's colour from blue to red.
Reprinted with permission from [77]. ©(2009) American Institute of Physics.

mations, assuming T–T annihilation to be the only T decay channel at large current densities, do not provide satisfactory agreement for the experimentally measured roll-off (see e.g. Fig. 10c, curve for 1%PtOEP:CBP) and, moreover, they are unable to predict the low current densities increase of the EL yield (see Fig. 10a). The reason lies in the incorrect assumption $P_R = P_d = 1$ (for definitions see Eq. (3)), that is, the neglection of the current-induced reduction of the recombination time (thus an increase of P_R) and electric field-induced reduction of the triplet lifetimes due to dissociation (thus a decrease of P_d). Their role is discussed later on in Section 5 dealing with the EL of EXLEDs.

In contrast to the PtOEP-doped PHOLEDs, doped PHOLEDs based on the highly efficient NĈN̂-coordinated complexes PtL^nCl, of the type shown in Fig. 9i, show monomolecular EL spectra with well-resolved structure and, due to optimized architecture, very high overall EL QE [77]. The EL spectra of devices prepared with a selection of four such complexes doped (5 wt%) into TCTA as the EML are shown in Fig. 11, together with the device architectures and structural formulae of the complexes. The well-resolved EL spectra fall in the bluish-green region of the visible spectrum, the spectra for the F-substituted complexes being slightly blue-shifted. Fig. 12 shows the PHOLEDs' colour quantified by CIE coordinates (cf., Section 2.2). The EL from PtL^{23}Cl-based EML gives the most blue-shifted spectrum with CIE coordinates (0.18, 0.35) but appears to be extremely sensitive to the concentration, the PHOLED colour shifting up to the red at high loadings. This is associated with a change in the EL spectrum caused by the formation of excimers and will be discussed in Section 5. At the same time, this PHOLED reveals the highest EL QE, reaching 18.3% at 10 wt% concentration, partly due to the high phosphorescence efficiency of the complex itself. For photophysical parameters of the PtL^nCl complexes in question, see Table 1.

Judicious choice of PHOLED architecture contributes substantially to improvements in EL efficiency. As shown in Fig. 11, the devices consist of an ITO-coated glass anode transparent to the light generated in the EML. Holes are injected from the ITO anode, and pass through TPD:PC and TCTA hole-transporting layers, and recombine in the EML with electrons that were injected from an Al/LiF cathode and transported through the electron-transporting layer of TAZ. The 10 nm-thick TCTA layer, characterized by a

Table 1
Photophysical and electrochemical parameters of the PtL^nCl complexes in solution and neat solid films.

Pt complex	φ_{PL} (%)	τ (μs)	E_p^{ox} (V) vs SCE[c]	E_p^{red} (V) vs SCE[c]
PtL^{21} Cl				
Solution	73[a]	6.8[a]	–	–
Film	5[b]	0.2	–	–
PtL^{22} Cl				
Solution	85[a]	13.6[a]	0.73	−1.86
Film	35[b]	1.0	HOMO = 5.41[d]	LUMO = 2.82[d]
PtL^{23} Cl				
Solution	87[a]	7.9[a]	0.75	−1.80
Film	65[b]	2.4	HOMO = 5.43[d]	LUMO = 2.88[d]

[a] Photoluminescence data (φ_{PL}, τ) in DCM solution at 295 K.
[b] Calculated using standard BASF LumogenF Red.
[c] Electrochemical data in DMSO solution. Irreversible potentials are reported.
[d] HOMO and LUMO levels (eV) calculated from the solution redox potentials.

triplet exciton energy E_T of 2.85 eV, has been used to block triplet exciton transfer from the Pt complexes ($E_T < 2.6$ eV) to the non-radiative triplet of TPD ($E_T = 2.45$ eV). The 30 nm-thick layer of TAZ ($E_T = 2.75$ eV) plays a similar role of inhibiting quenching of the Pt complex triplet excitons at the cathode while at the same time blocking holes, both properties that enable the recombination process to be confined to a 30 nm-thick EML layer. Such a PHOLED architecture allowed us to maximize its performance parameters (for general mechanisms of PHOLED function see e.g. Ref. [8]). The variation of the external EL QE with density of the driving current differs for PtL^{n}Cl according to the substituents in L^n (Fig. 13a). The functional shape of the evolution resembles that for PtOEP (see Fig. 10) and can be explained, as previously, on the basis of the unified approach expressed by Eqs. (2) and (3). A quantitative description of EL QE vs j will

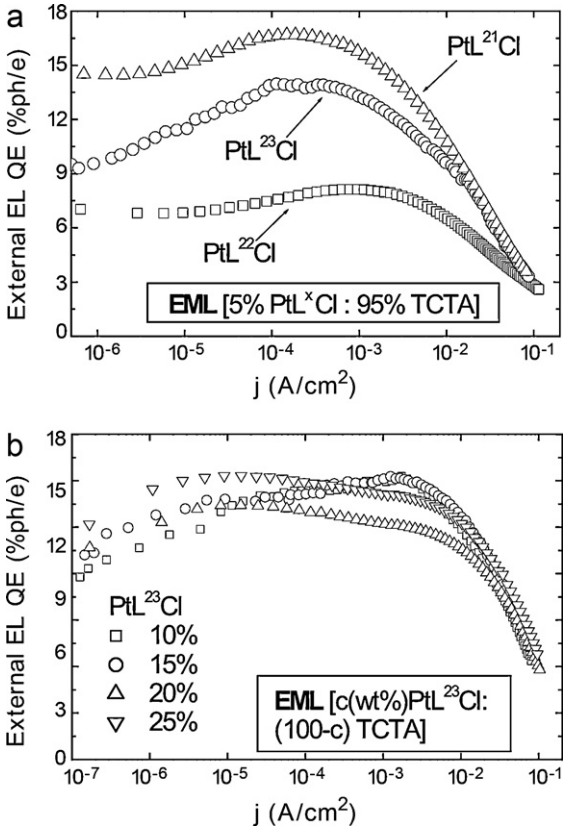

Fig. 13. (a) External EL QE of selected PtL^nCl-doped PHOLEDs. (b) External EL QE of the PtL^{23}Cl device at varying dopant concentration.

be presented in Section 5. Only minor differences are observed in the j evolution of EL QE with varying dopant concentration (Fig. 13b).

5. Excimer and exciplex OLEDs (EXLEDs)

Organoplatinum(II) complexes appear to be excellent emissive compounds for OLEDs also because of their distinctive ability to form bi-molecular (B-M) excited states (cf., Section 2.4) which, due to their high radiative decay, allow the manipulation of both the OLED's colour and efficiency. Mostly, excimers are generated in single-component EMLs and exciplexes in electron-donor (D) and electron-acceptor (A) bi-component EMLs using Pt(II) organic complexes (for a recent overview see e.g. [78]). The OLEDs featuring emission from such B-M excited states have been named EXLEDs (cf., Section 2.6). Recently, highly efficient, variable-colour PHOLEDs have been realized via mixing of molecular exciton and excimer phosphorescent emissions from PtL^{26}Cl (Fig. 9i, X = F, R = 4-OMe) [5]. PtL^{26}Cl-doped TCTA blends have been used as either the low-concentration bluish green (molecular) phosphorescence emitter or high-concentration red (excimer) phosphorescence emitter. By adjusting the relative amount of blue and red emissive species, the colour of the light emission was tuned from bluish-green through green and white up to red as shown in Fig. 14. The concentration-optimized devices, with the architecture as presented in Fig. 11, can easily reach high brightness up to $L = 10{,}000\ \mathrm{cd/m^2}$, achieving extremely high external quantum efficiency (EQE) up to 20% at low current densities ($<10^{-2}\ \mathrm{mA/cm^2}$) and up to 17% at $L = 500\ \mathrm{cd/m^2}$. High purity white light emission [CIE coordinates ($x = 0.34$, $y = 0.35$)] was realized at this luminance, QE = 11.5%, power efficiency of 6.8 lm/W and colour rendering index (CRI) = 74, though CRI = 81 has been achieved with CIE coordinates ($x = 0.42$, $y = 0.38$). These performance data are among the best achievements reported for colour and white emission organic LEDs (cf., Section 6). As far as the theoretical fit to the current density evolution of EQE is concerned, the situation becomes here more complex because two types of the emissive species, molecular excitons and excimers, have to be accounted for in the general formula of Eq. (2) [11]. This requires the determination of the relative contributions of the monomer blue and excimer red emission bands (see Fig. 14) and information on some microscopic parameters for the EML, such as the lifetimes and phosphorescent yield of the emissive states or electron- and hole-mobilities and their hopping distance within the emitter. Such a fitting procedure has been performed based partly on independently measured parameters (lifetimes and phosphorescent efficiencies) but some others treated as fitting parameters (charge-carrier transport data) [11]. The result is shown in Fig. 15. The theoretical curves reproduce the experimental data quite well, proving that the general approach to the quantum efficiency of OLEDs, expressed in Eqs. (2) and (3), can be correctly applied even to the complicated multi-center emitters like {PtL^{26}Cl(x):TCTA($100 - x$)}. We note that it is P_R which is responsible for the EQE increase in the low current density region; the remaining two possibilities, P_d and P_q, decrease monotonously with increasing current density and have a decisive effect on the EQE(j) curve at large current densities (Fig. 15b). At least two aspects of the EQE(j) behaviour should be highlighted. Firstly, it provides an interesting tool for the verification of the experimental data using independently obtained optical and charge transport parameters or, if they are not available from independent experiment, can serve as a way of determining them by an optimal overall fit of EQE(j) to the EQE experiment; secondly, it includes the impact of OLED architecture through the charge-carrier injection conditions at the interface between the component materials, determining the ratio of the one-carrier SCL current (j_{SCL}) to that driving the device (j) (cf., Fig. 15c).

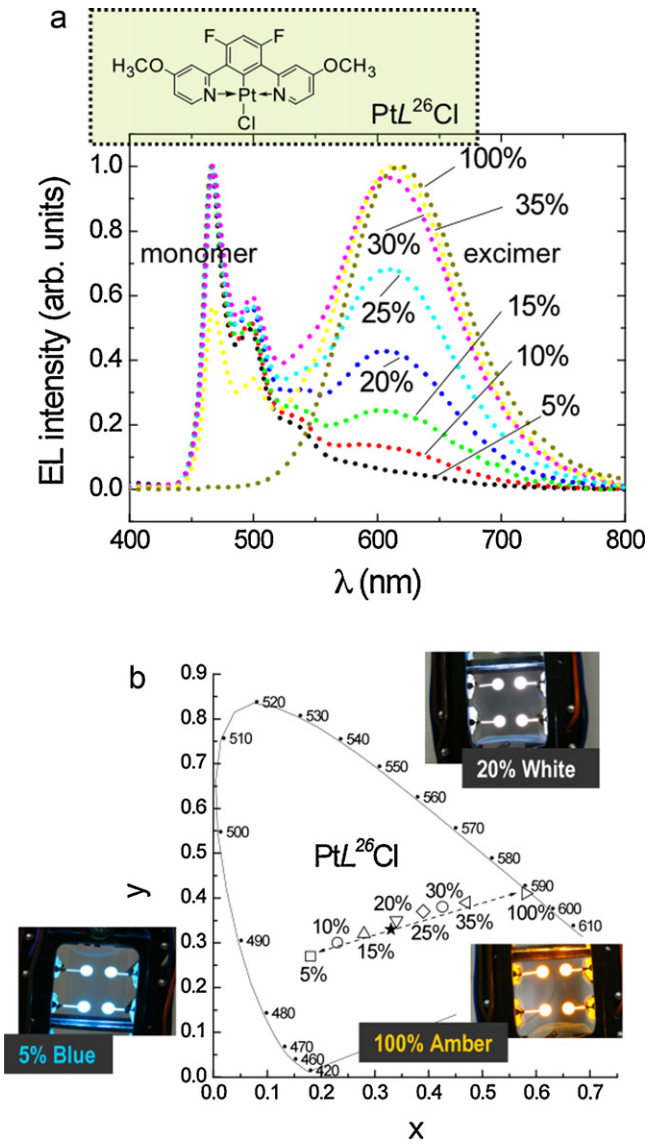

Fig. 14. EL spectra (a), and CIE diagram showing (x, y) colour-coordinates (b) for OLEDs with emitters of varying concentrations of PtL^{26}Cl. At low concentrations of the phosphor, the OLEDs are "blue-biased" (dominated by emission from the molecular triplet excitons) which fall into the PHOLED category; at high phosphor concentrations the LEDs become "red-biased" being dominated by the emission from phosphor excimers, and they fulfil criteria to fall in the EXLEDs category. The blue emission band practically disappears for 100% phosphor emitter (neat PtL^{26}Cl films). The LED with a 20 wt% content of the phosphor closely approaches white light with CIE coordinates ($x = 0.33$, $y = 0.33$). Examples of emission colours at various phosphor concentrations are given by photographs in the CIE diagram in part (b).
Reprinted with permission from [5]. ©Elsevier.

A two-component EML composed of electron-donor (D) and electron-acceptor (A) molecules is used to form exciplex OLEDs, another sort of EXLEDs. The emission from singlet and triplet exciplexes can be observed. The exciplex singlet-to-triplet fraction appears to be a function of electronic properties of the (D–A) complex molecular components, their separation, and the applied electric field [79]. The energy level relations between an electron donor (m-MTDATA) and a number of electron acceptors, including PtL^2Cl (a complex of the type shown in Fig. 9i, R = X = H, carrying a CO_2Me group at the phenyl position *para* to the metal), along with their PL spectra are displayed in Fig. 16. The formation of exciplexes

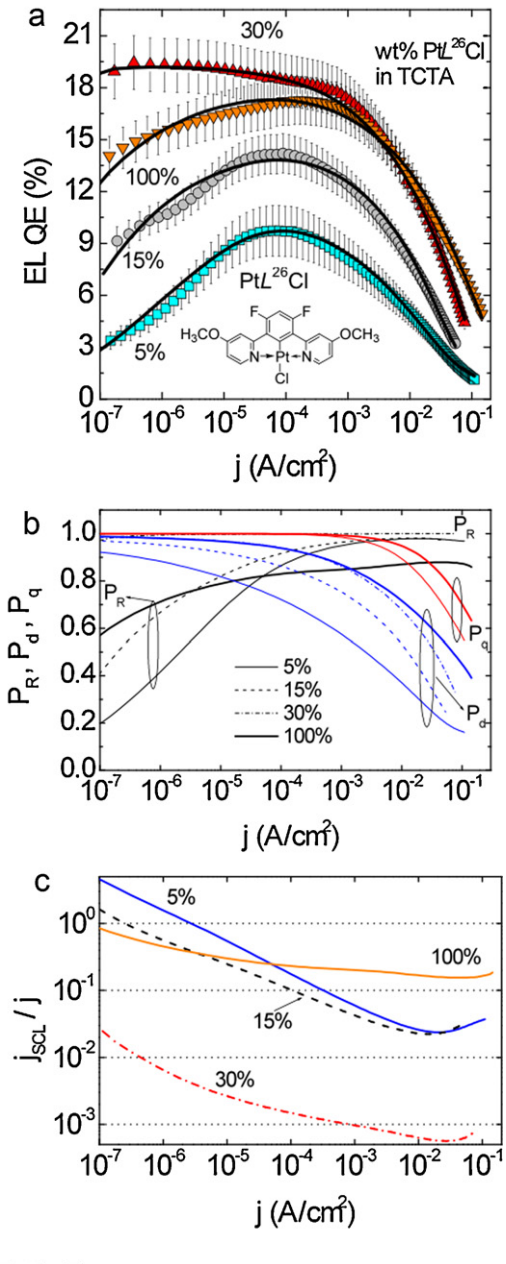

Fig. 15. (a) Selected experimental data points of the external ELQE vs device current density for the devices with four different concentrations of PtL^{26}Cl as indicated in the figure (cf. Fig. 2); and the corresponding theoretical curves based on Eq. (2) and the current evolution of P_R, P_d and P_q from part (b) (solid lines). (b) The recombination (P_R), dissociation evasion (P_d), and quenching escape (P_q) probabilities defined by Eq. (3) as a function of current density at different dopant concentrations, c_1 = 5 wt%, c_2 = 15 wt%, c_3 = 30 wt% and c_4 = 100%. The values of fitting parameters are given in the text. (c) The calculated space-charge-limited hole (hole + electron) current/measured current ratio (j_{SCL}/j) vs j.
Reprinted with permission from [5]. ©Elsevier.

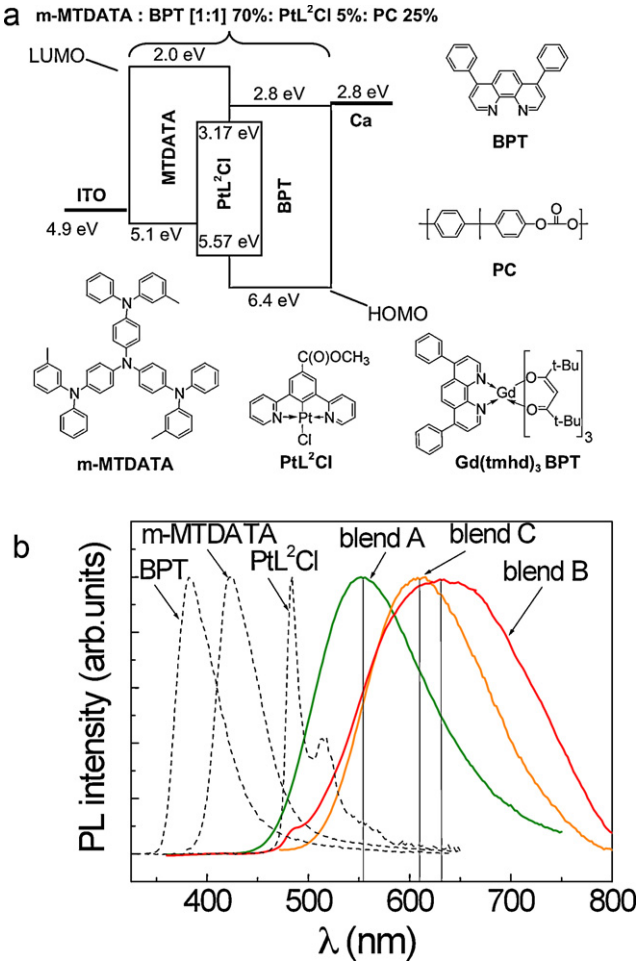

Fig. 16. (a) Energy level diagram of the blends and molecular structures of the materials used for different exciplex emission-based EXLEDs. Two blends have been prepared: undoped (Structure A) and doped with a phosphor PtL^2Cl (platinum (II)[methyl-3,5-di(2-pyridyl) benzoate] chloride) (Structure B) of m-MTDATA (4,4′,4″-tris(*N*-(3-methylphenyl)-*N*-phenylamino) triphenylamine):BPT (bathophenanthroline):PC, donor (m-MTDATA) and acceptor (BPT) system blended with a polycarbonate (PC) electronically neutral binder. (b) Normalized PL spectra of structures (A) and (B) to be compared with the PL spectra of their material components: fluorescence of m-MTDATA and BPT, and phosphorescence of PtL^2Cl along with an exciplex phosphorescence spectrum for a [m-MTDATA:Gd(tmhd)$_3$BPT] film (blend C).
Reprinted with permission from [79]. ©Elsevier.

is clearly seen from the PL spectra shown in Fig. 16b. While the PL spectra of individual materials (monomolecular fluorescence of m-MTDATA and BPT, and phosphorescence of PtL^2Cl) are relatively narrow (and well structured in the case of PtL^2Cl), the broad-band emission from their blends (m-MTDATA:BPT[1:1] 70 wt%:PC 30 wt%) (A), (m-MTDATA:BPT[1:1] 70 wt%:PtL^2Cl 5 wt%:PC 25 wt%) (B), are characteristic of singlet $^1|$m-MTDATA : BPT$\rangle^*$ and triplet $^3|$m-MTDATA : PtL^{2}Cl$\rangle^*$ exciplex emission peaking at 560 nm and 635 nm, respectively. The PL spectrum centred at ≈605 nm for the blend [m-MTDATA:Gd(tmhd)$_3$BPT] (C) originates from the triplet exciplex $^3|$m-MTDATA : Gd(tmhd)$_3$BPT$\rangle^*$. The efficiency of EXLEDs has been shown to be greatly improved by the introduction of a Pt complex acting as a phosphorescent sensitizer with a high electronic affinity (Fig. 17) [80]. The EQE of the double-layer (DL) EXLED with an EML made of PtL^2Cl-containing blend B [ITO/EML (blend B)/ETL (BPT)/Ca)] is roughly double that with no sensitizer A, reaching a maximum value of (2.4 ± 0.1%). A completely different behaviour of the non-PtL^2Cl-doped blend EML (A) single-layer (SL) EXLED should be pointed out. Its EL spectrum is strongly red-shifted and the PL decay time much longer with respect to those for the DL EXLED with the same EML. Though both SL and DL device EL spectra (and corresponding PL spectra of their EMLs) are broad suggesting their exciplex origin, the difference in the wavelength location and PL decay times allow to their differing spin multiplicities to be inferred: the DL EL originates from singlet ($h\nu^{(1)}$) and SL EL from triplet ($h\nu^{(3)}$) exciplexes. The explanation for this unusual observation is associated with an important topic of the spin multiplicity of the ($D^+ \ldots A^-$) pairs preceding the final exciplex states.

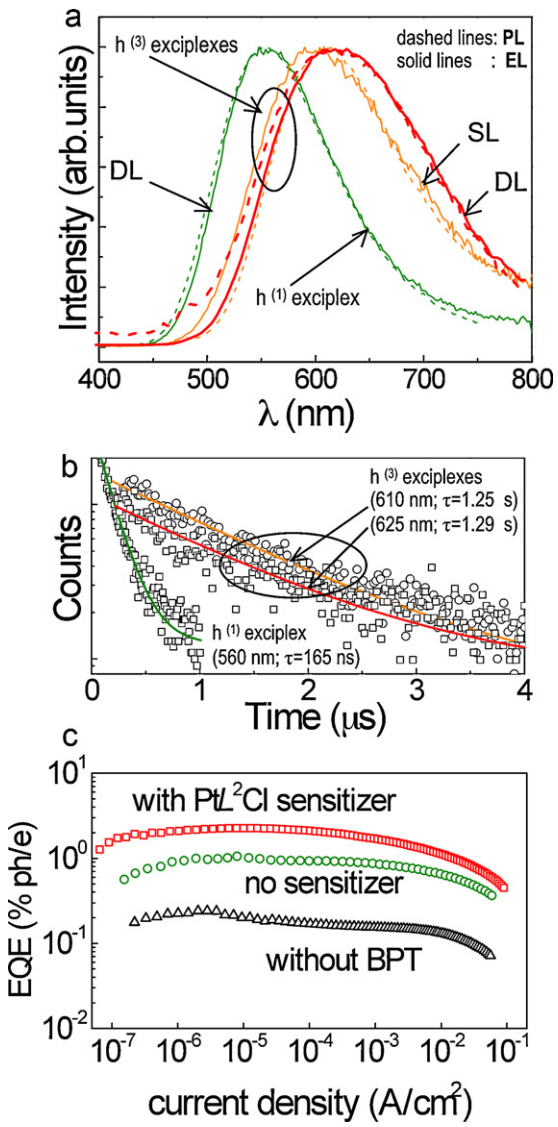

Fig. 17. (a) Singlet [$h\nu^{(1)}$] exciplex spectra recorded under optical (PL) and electrical (EL) excitation of the emitting layers of device I based on blend A. The exciplex phosphorescence emission spectrum $h\nu^{(3)}$ has been measured for a [m-MTDATA:Gd(tmhd)$_3$BPT] and [m-MTDATA:PtL^2Cl:BPT:PC] film excited by light (PL) at 350 nm (orange and red dashed lines). The EL spectrum of a single-layer (SL) LED (ITO/m-MTDATA:BPT:PC/Ca) is added to compare with that of the double-layer (DL) structure of device (I) and (II), the latter based on PtL^2Cl-doped blend B. (b) PL decay curves at the maxima of the fluorescence (560 nm) and phosphorescence (610 nm, 625 nm) exciplex spectra excited at 336 nm under argon atmosphere; the decay times, τ, are given in the parentheses along with the location of the emission maxima. The decay time for $h\nu^{(3)}$ decreases by about 30% in ambient air (not shown in the figure). (c) EL quantum efficiency (QE) of the EXLED devices (I) and (II) demonstrating the effect of PtL^2Cl doping. At $j \cong 0.01$ mA/cm^2, the QE reaches a maximum value of (2.4 ± 0.1)% photon/carrier for the sensitized structure (II). The EL QE for the emitting layer of (m-MTDATA:PtL^2Cl:PC) without BPT is added (triangles), showing the acceptor (BPT) role in transporting electrons to PtL^2Cl trapping centres.

In contrast with the commonly held view of purely statistic basis for the excitonic singlet–triplet ratio (1:3) (cf., Fig. 4), this ratio can differ if the singlet–triplet intersystem crossing (ISC) rate is competitive with the rate of exciton formation. The ISC rate (k_{ISC}) is a function of the singlet–triplet charge pair (CP) gap, ΔE_{ST}, which is a strongly material-dependent quantity [81,82]. If ΔE_{ST} is sufficiently large, k_{ISC} will be as a rule very slow relative to both the formation rates of triplet and singlet excitons and the resulting singlet-triplet exciton formation ratio will be 1:3. Meanwhile, for small ΔE_{ST} values, k_{ISC} becomes large enough to increase this ratio to such a degree that the fluorescence efficiency will exceed that of phosphorescence. At the short interion ($D^+ \ldots A^-$) distances, the spin–spin exchange interaction is dominated by kinetic exchange, which favours the singlet state. Moreover, for larger initial interion distances, coulombic interaction within the CP ($D^+ \ldots A^-$) state causes reorganization that decreases the distance between the electron and hole and further increases the singlet-favouring kinetic exchange [82]. In an extreme case of a very strong exchange interaction (short distances and energy-favoured orientation of the ions), the quasi-complete CP triplet-to-singlet conversion eliminates the formation of triplets, and only fluorescence will be observed. This reasoning can be extended to the fluorescence and phosphorescence of the exciplexes as demonstrated in Fig. 17. The green EL emission of the PtL^2Cl-undoped DL EXLED originates mainly from the singlet exciplexes ($h\nu^{(1)}$) formed at the (blend (A)/BPT) interface, whereas the red EL emission of the SL EXLED emanates mostly from the triplet exciplexes ($h\nu^{(3)}$) generated efficiently in the bulk of EML made of the same blend. The difference in the exciplex spin multiplicity is due to different environmental conditions at the interface and in the bulk of the emitter. The interface recombination ($D^+ \ldots A^-$) favours the formation of singlet exciplexes since the interface dipolar layer ($D^{+\alpha e}/A^{-\alpha e}$) – where αe is the partial charge transferred from D to A because of the difference in their electronegativity – creates a potential facilitating the formation of a closer located ionic species of the singlet exciplex rather than triplet at larger equilibrium exciplex separation [83]. In the emitter bulk of the SL EXLED, the formation of triplet exciplexes is dominating due to, on average, more widely spaced D–A molecules (compared with the interface distance). The concentration of singlet exciplexes is negligibly low as discussed above in the context of the ISC rate (k_{ISC}) dependence on the singlet–triplet charge pair (CP) gap, ΔE_{ST}. The sensitised emission mechanism of the PtL^2Cl-doped EML-based DL EXLED is due to the conversion of the interfacial electron-hole recombination in the fluorescent undoped EXLED to the bulk recombination in the EML, where the formation of triplet exciplexes is preferred on the PtL^2Cl$^-$ recombination centres, leading to efficient dopant exciplex phosphorescence.

5.1. Near-infrared OLEDs (NIROLEDS)

The extension of efficient OLEDs into the technologically important near-infrared (NIR) spectral range (NIROLEDs) poses another challenge to scientists and engineers. Various approaches have been explored to obtain infrared emission from organic LEDs. The use of rare earth complexes and small optical gap polymers has been attracting interest since lanthanide ions such as Er^{3+} or Nd^{3+} emit in the NIR, and the polymer emission extends to a wavelength of 1000 nm. One of the most important shortcomings of the NIROLEDs is poor quantum efficiency and low power output. For example, forward light output of 100 μW/cm^2 and only 0.1% of external quantum efficiency have recently been reported for NIR electrophosphorescence, with a peak value at 720 nm, from blends of polymeric host and an iridium (III) complex [32]. A dispersion of inorganic indium arsenide-based nanocrystals in conjugated polymers has been employed to improve the quantum efficiency but to no more than ≈0.5% ph/e [33] comparable with 0.3% for a NIROLED using multimetallic assemblies of lanthanides and iridium complexes at the maximum emission wavelength 1060 nm [84]. Notable progress has been reported using Pt(II) tetraphenyltetrabenzoporphyrin, Pt(TPBP), as dopant in Alq_3 EML, the emission peaking at 772 nm with an EQE of 8.5% at very low current densities $<4 \times 10^{-6}$ A/cm^2 [85]. Recently, the application of excimer phosphorescence from neat films of cyclometallated Pt(II) complexes has enabled the fabrication of highly efficient NIROLEDs (up 14.5% ph/e) [86,87], opening up a new perspective for further improvements in this important branch of optoelectronics, as highlighted

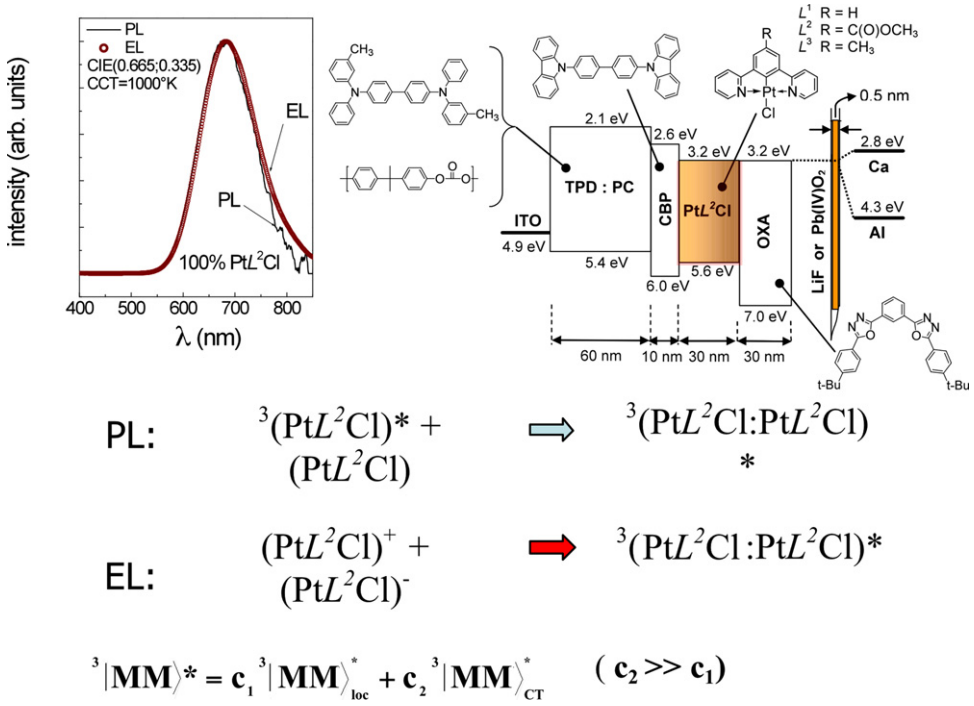

$$^3|MM\rangle^* = c_1\,^3|MM\rangle^*_{loc} + c_2\,^3|MM\rangle^*_{CT} \qquad (c_2 >> c_1)$$

Fig. 18. Red/near-infrared excimer LEDs using Pt(II) complexes with various substituents L^n (here a PtL^2Cl-based LED is demonstrated). Two different pathways of formation of excimer triplets in PL and EL are pointed out (cf., Section 2.4). The CIE and CCT of the emission are shown aside the PL and EL spectra.
Adapted from [87].

in an article entitled *High-Efficient Organic LEDs Extended to Near-IR* in Europhotonics Magazine (February–March 2007). An example of a highly efficient NIROLED based on phosphorescent molecules of PtL^nCl is shown in Fig. 18. Its neat film PL and EL spectra coincide, peaking at about 700 nm, suggesting that CT triplet excimers dominate the emission. As shown in Fig. 18, such films can form an emission layer in a four-layer LED, layers of CBP and OXA confine the recombination and emission to the emitter layer, due to their blocking function for suitable charge carriers and triplet excitons. Changing the ligand allows the spectrum to be red shifted as illustrated in Fig. 19a. The emission maximum for a hydrogen atom as a ligand is located at about 720 nm, the NIR region, above 700 nm covers roughly a 50% of the whole spectrum with still high quantum efficiency. These LEDs exhibit the highest up to date quantum efficiency in the NIR region. It exceeds 9% ph/e for all buffer layers in front of the cathode, and reaches almost 15% ph/e for a lead (Pb) oxide buffer (Fig. 19b).

6. White light emitting OLEDs (WOLEDs)

Among the most rapidly developing classes of OLEDs, white-light-emitting-diodes (WOLEDs) are of particular interest because they offer low-cost alternatives to back-lights in flat panel displays and are considered as future illumination sources which are able to operate at low voltages with high luminance efficiency [8,88]. By definition, the emission spectrum of WOLEDs must cover unequivocally the whole of the visible part of the electromagnetic spectrum. Several routes have been employed to realize this goal. The fabrication of stacked [2] or multilayer [89,90] LED structures with separated molecular emitters, that is blue, green and red, was proposed initially. Other approaches involve stacked RGB emitters [91], fluorescent/phosphorescent emitters [92], multiple fluorophore or multiple phosphor-doped emitters [93–95], phosphorescent triple-doped emitters [96] or exciplex emission with mixed acceptors [97]. However, the WOLEDs with the most impressive characteristics are those based on a single emissive

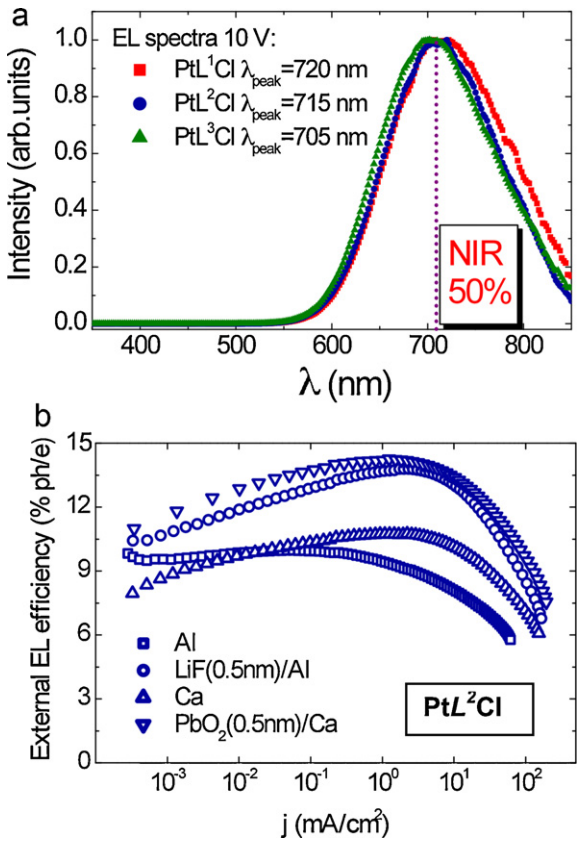

Fig. 19. (a) The EL emission spectra from neat films of PtL^nCl with different ligands [86] as indicated in Fig. 18. (b) The EL external quantum efficiency as a function of driving current of a LED based on a neat film emitter of PtL^2Cl with different buffers at the cathode [87]. The LED architecture as given in Fig. 18.
Adapted from [86,87].

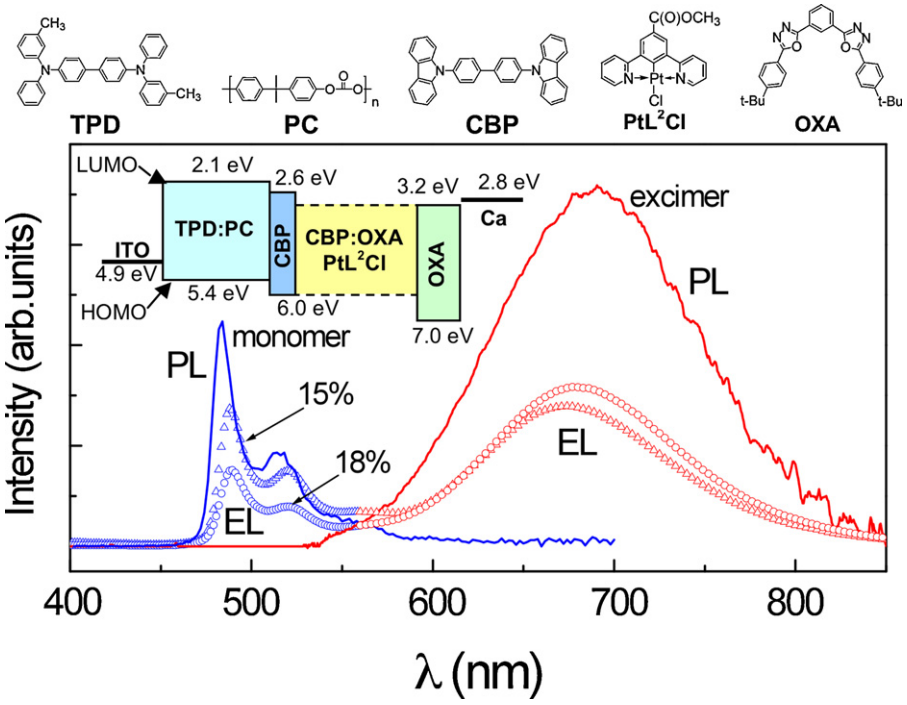

Fig. 20. Normalized monomer (blue figures) and excimer (red figures) EL spectra at two different PtL^2Cl concentrations of the device shown in the inset. Indicated are the lowest unoccupied molecular orbital (LUMO) energies and the highest occupied molecular orbital (HOMO) energies of the materials used. Top: the molecular formulae of TPD, PC, CBP, PtL^2Cl and OXA. The photoluminescence (PL) spectra of low-doped (5%) samples (solid blue line) and a 100% (solid red line) evaporated PtL^2Cl film are shown for comparison.
Reprinted with permission from [87]. ©(2009) American Institute of Physics.

dopant, where molecular excitons are harnessed to form triplet excimers [93,98,99] or/and exciplexes [100] in addition to molecular (monomolecular) excited states.

For instance, varying the concentration of PtL^2Cl in PtL^2Cl-doped CBP:OXA EMLs has been shown to differentiate the ratio of the bluish-green monomer to red excimer components as depicted in Fig. 20, revealing their mixing to generate different colour OLEDs (for another Pt(II) complex-doped OLEDs with similar behaviour cf., Fig. 14). The ratio of monomer/excimer contributions is quasi-invariant with applied voltage, and white light from a balance of monomer and excimer emissions is observed for devices with PtL^2Cl-doped emitters between 10 and 20 wt%. Examples are shown in Fig. 21. The CIE coordinates $x = 0.43$ and $y = 0.43$ for the 15%-doped device are close to those in an incandescent lamp, approximately $x = 0.41$ and $y = 0.41$. At a higher concentration (18 wt%), the CIE coordinates (0.47, 0.41) are shifted to the red as compared with those for an incandescent lamp. The peak brightness at ≈80 mA/Cm^2 of the 15%-doped device is 7000 cd/m^2 and a maximum EQE is $15.5 \pm 0.2\%$ (14.2 ± 0.2 cd/A) at 10 cd/m^2, showing only a small drop to 13.5 ± 0.2 (12.6 ± 0.2 cd/A) at 1000 cd/m^2. While the brightness is comparable with the best reported data for single-dopant WOLEDs, the emission efficiency exceeds them by a factor of about 5 [94,96]. They clearly make these devices most suitable for use as white light illumination sources. The emission efficiency of two of them with two different concentrations of PtL^2Cl vs current density is shown in Fig. 21b. The quantum efficiency decreases at high current densities; however, the decrease is less severe than in most other electrophosphorescent devices [75,76], including single dopant WOLEDs [93,96,101]. Less than 50% drop of the maximum EL quantum efficiency at 100 mA/cm^2 is observed, compared to a roll-off of three to four-fold for the other most efficient single dopant WOLEDs reported hitherto [93,96]. This is another advantage of these WOLEDs, resulting from the reduced sensitivity of emissive states to quenching by their mutual interaction, fate of charge carriers and electric field-enhanced dissociation (see Section 2.2).

Recently, a high-performance organic WOLED based on a Pt(II) complex with a high CRI = 90 has been fabricated that exploits three different emissive species mixed together in one emissive layer to get stable colour balance at a high external electroluminescence quantum efficiency and correlated colour temperature CCT = 3067 K [100]. Its architecture and performance characteristics are presented in Fig. 22. The overall EL spectrum of this WOLED is composed of three essential bands corresponding to the photoluminescence (PL) spectra of molecular triplet emission of PtL^2Cl (green line 2), triplet exciplex emission of m-MTDATA:PtL^2Cl (orange line 3) and excimer emission of PtL^2Cl (red line 4) with a small blue contribution from the molecular singlet emission of TPD, $^1D^*$. They appear as a number of characteristic features in the EL spectrum. Their percentage contribution to the EL spectrum by the area under the curves is given in part (b) of the figure. Performance characteristics of selected most advanced organic WOLED structures are listed in Table 2. The highest efficiency systems (12% and 15.5%) give CIE coordinates close to those found in incandescent lamps (*ca.* 0.41, 0.41). The systems with the highest CRI, 90 and 90.4, place the device colours at the warm and pure white light points, respectively. We note that among the three EL systems with the highest efficiency and CRI, two are based on phosphorescence from Pt(II)-based WOLEDs.

7. Plant growth OLEDs (PGOLEDs)

High-brightness, low energy-consuming light sources are anticipated that will optimize plant growth through the photosynthesis process. Only a relatively small amount of solar radiation – in the visible region – is used by plants for growth, referred to as growth

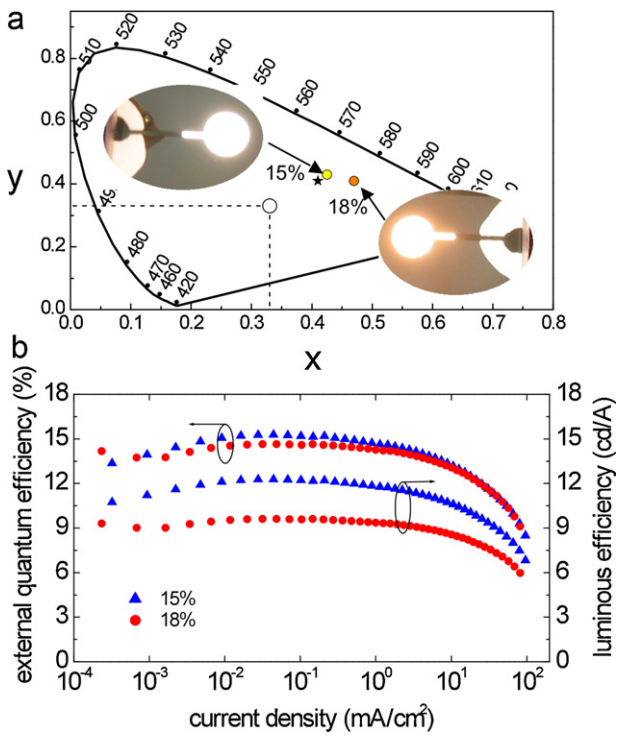

Fig. 21. (a) CIE chromaticity diagram for the WOLED ITO/TPD:PC/CBP/CBP:OXA:*n*%PtL²Cl/OXA/Ca. The photos show the combined monomer + excimer emission for devices doped at 15 and 18 wt%. The dots refer to the colour points of the emission spectra of the devices with these two different concentrations of PtL²Cl. Concentrations close to 15% gave the CIE coordinates closest to white (0.33, 0.33) (open circle) and those found in soft light incandescent lamp (*ca.* 0.41,0.41) (asterisk). (b) Luminous and external EL quantum efficiency vs current density for the WOLEDs with optimized concentrations of the phosphor. The photon energies have been averaged over the complete emission spectra and Lambertian intensity profiles assumed in the calculation of the external quantum efficiency of each device.

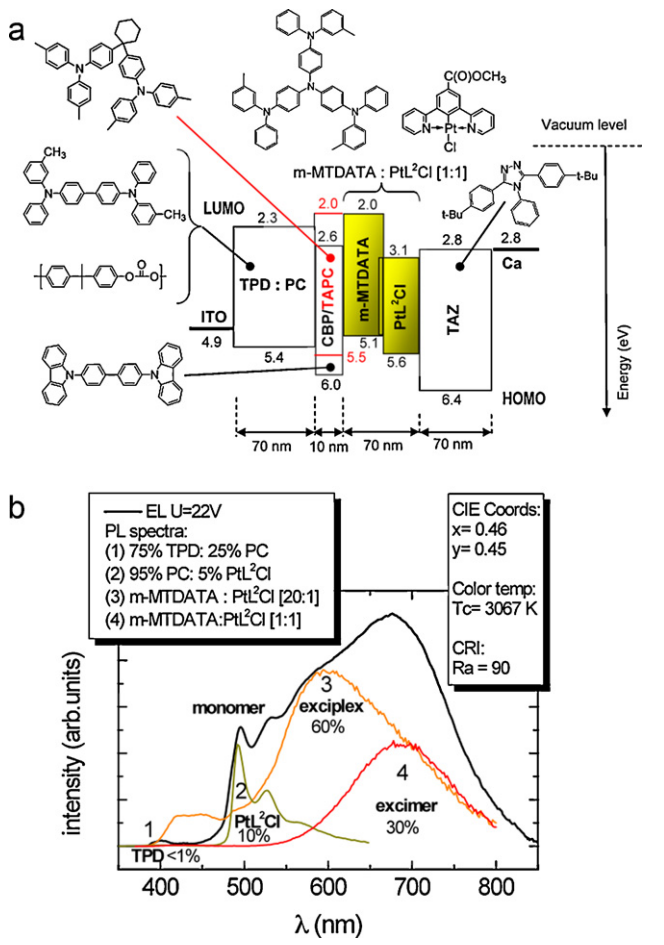

Fig. 22. (a) The architecture of a single-dopant, Pt*L*²Cl, WOLED mixing the molecular, excimer and exciplex emissions in one EML. Molecular structures of the materials used are given around the device scheme. The highest occupied molecular orbital (HOMO) obtained for each material corresponds to its ionization potential. The lowest unoccupied orbital (LUMO) is equal to the molecular electronic affinity. The Fermi level positions for ITO and Ca electrode contacts are added for completion. The positions of all the levels are indicated by the numbers in electronvolts relative to the vacuum level at energy zero. (b) The electroluminescence spectrum (black line) for the device, recorded at a voltage of $U = 22$ V. It is composed of three essential bands corresponding to the photoluminescence (PL) spectra as shown by lines 1, 2, 3, 4 for the systems indicated in the upper-left corner inset and described in the text. Some performance parameters, CIE coordinates, CCT, and CRI are given in the upper right corner inset.
Reprinted with permission from [98]. ©(2007) Wiley.

light. When a supplemental, artificial light is used to enhance growth, its source should ideally produce growth light efficiently. With the development of ever-improving LEDs for lighting over the last decade, it is finally becoming economical to use LEDs as growth lights (cf. the NASA LED ultimate grow light). They can be used in any application – hydroponics or soil, home or greenhouse. Researchers of NASA's Kennedy Space Center are working on the application of LEDs in the fabrication of a salad machine that could enable space center crews to grow and harvest their own greens within the next three years.

A typical inorganic LED is usually a small area source that emits an incoherent narrow-spectrum with the colour dependent upon the composition and condition of the semi-conducting material used. To convert such point light sources into solid-state lighting (SSL) lamps, creating a uniform and homogeneous light output, it is necessary to use optics which increase the weight and require more space for the lighting systems. In contrast, organic LEDs for SSLs represent a diffuse source of light and so they are naturally suited to large area general-lighting required for growing plants. The spectral distribution of light is one of the most important variables for

Table 2
Most advanced, selected performance characteristics of organic WOLED structures.

Structure	φ_{ext} [% ph/e]	η_P [lm/W] (L) [cd/m²]	CIE[a]	CRI[b]	Comments and references
Fluorescent/phosphorescent	11.0	22.1 (500)	(0.38, 0.41)	85	Maximum values [59]
Multiple phosphor-doped emitters	5.2	6.4	(0.37, 0.40)	83	Maximum values [60] (L is not specified)
Phosphorescent triple-doped	12.0	26.0 (100)	(0.43, 0.45)	80	Values at 10^{-3} mA/cm² [34]
Phosphorescent triplet excimers	5.7	5.2 (500)	(0.40, 0.43)	81	Maximum values [61]
	15.5	9.5 (40)	(0.43, 043)	<60	Maximum values [64]
	11.5	6.8 (500)	(034, 0.35)	74	Maximum values [5]
Phosphorescent triplet excimer/exciplex	6.5	9.0 (500)	(0.46, 0.45)	90	Maximum values [65]
Exciplex emission with mixed acceptors	–	– (425)	(0.32, 0.35)	90.4	No data for φ_{ext} and η_P are reported [62]

[a] CIE = Commission Internationale de l'Eclairage; ideal white light CIE coordinates are ($x = 0.33$, $y = 0.33$) and those for warm incandescent lamp light are (0.41, 041).
[b] CRI = colour rendering index; for ideal white light CRI = 100.

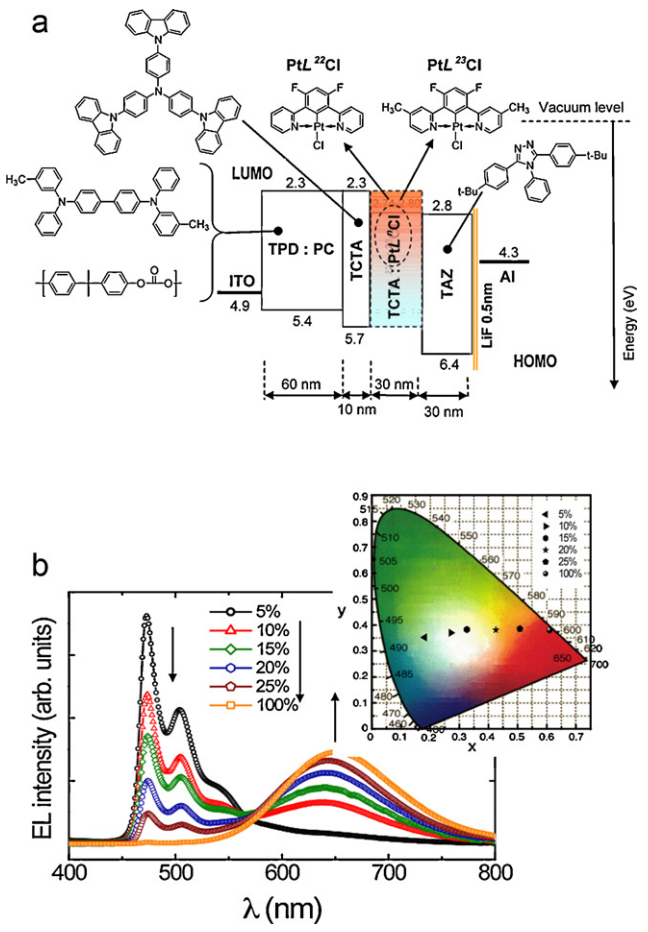

Fig. 23. (a) The architecture of the OLEDs and constitutent materials used to enable the devices to fulfil the spectral criteria for plant growth light sources (PGOLEDs). (b) EL spectra and CIE diagram (right-up corner inset) for OLEDs with emitters of varying concentrations of Pt*L*^{23}Cl. While the OLED with a 15 wt% content of the phosphor approaches closely a white light with CIE coordinates (0.33, 0.33), standing for a fairly good WOLED, the OLED with 20 wt% of Pt*L*^{23}Cl in the EML generates light with a characteristic resembling the action spectrum of photosynthesis (cf., Fig. 24a). Reprinted with permission from [38]. ©(2007) Wiley.

optimizing plant growth. Researchers have found that blue and red light is essential for plant growth. Therefore, the most desired characteristics of LED growth light are those combining emission bands in blue and red following the action spectrum of photosynthesis. The monomer and excimer emissions from single Pt(II)-complex-based phosphor dopant emitters have been proven to be effective in the creation of such two-band emission spectra (see Sections 5 and 6), and so such systems could be very promising for new plant growth light source technology.

A series of OLEDs that exploits the monomer and excimer emissions from single Pt(II) complex phosphor dopant emitters has been recently reported by us [40]. In Fig. 23a, the architecture of OLEDs able to fulfil the spectral criteria for the grow light source (PGOLEDs) is schematically presented. To achieve blue-to-red band proportions in the emission spectra of the LEDs corresponding to the action spectra of photosynthesis for different plants and their growth stage, control of the dopant concentration is crucial (Fig. 23b). An action spectrum is the rate of physiological activity related commonly to photosynthetic rate plotted against wavelength of light. Photosynthetic efficiency is rigorously defined as the amount of CO_2 fixed per absorbed photon, a ratio known as photosynthetic quantum yield, though the increase in plant dry mass is typically used as a more practical measure of physiological activity [102]. The rate of photosynthesis is related to the 'photosynthetic

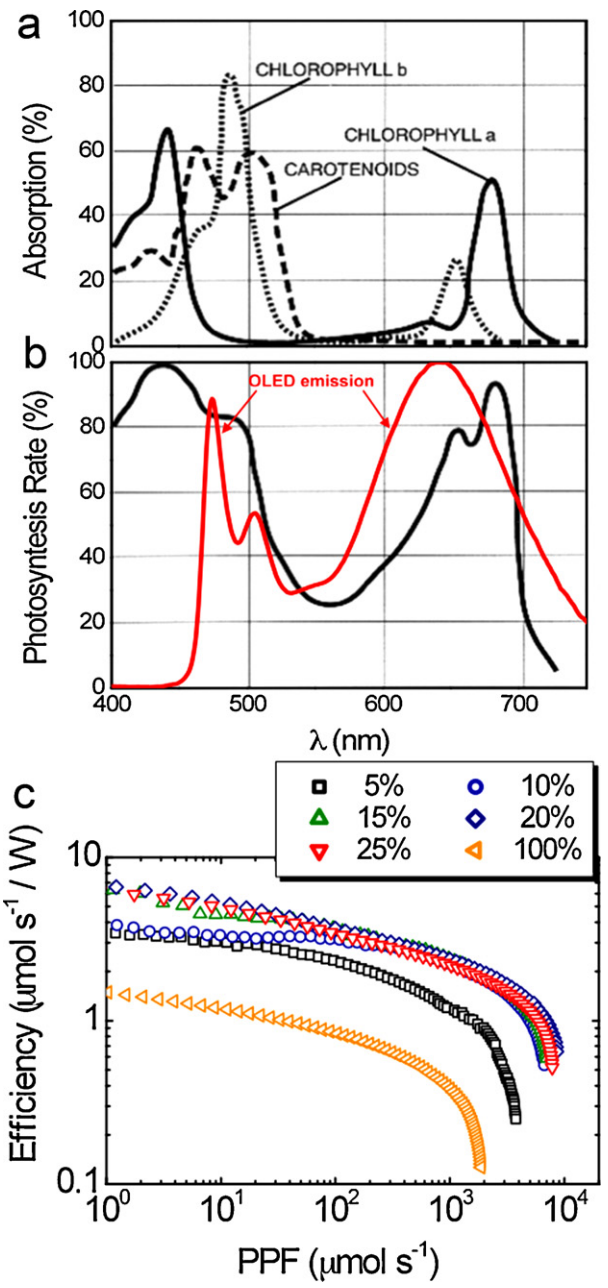

Fig. 24. (a) Absorption spectra of chloroplast chlorophyll-a and -b, and carotenoids, and (b) action spectrum of photosynthesis compared with the emission spectrum of one of the OLEDs (20 wt% in Fig. 23b). A remarkable correspondence between the OLED spectrum and the action spectrum (as taken from [100]) can be observed. (c) Growth light efficiency vs photosynthetic photon flux (PPF) referred to 1 m^2 emitting area of the device.
Reprinted with permission from [38]. ©(2008) Elsevier.

photon flux' (PPF) which is expressed by convention in μmol photons per second. Photosynthetic efficiency is routinely measured by determining the maximum quantum yield of plant leaves and is expressed by PPF absorbed per unit area of leaf (μmol × s^{-1} × m^{-2}). The higher the PPF value per Watt, the more efficient the light source for plant growth.

In Fig. 24 the spectrum of one of the OLED growth lights from Fig. 22b for 20 wt% Pt*L*^{23}Cl dopant EML (red solid line) is compared with the action spectrum of photosynthetic efficiency (black solid line). It is apparent that the peaks of the photosynthetic response curve follow roughly a combination of the absorption spectra of chlorophyll and carotenoids, a plant's primary energy-collecting

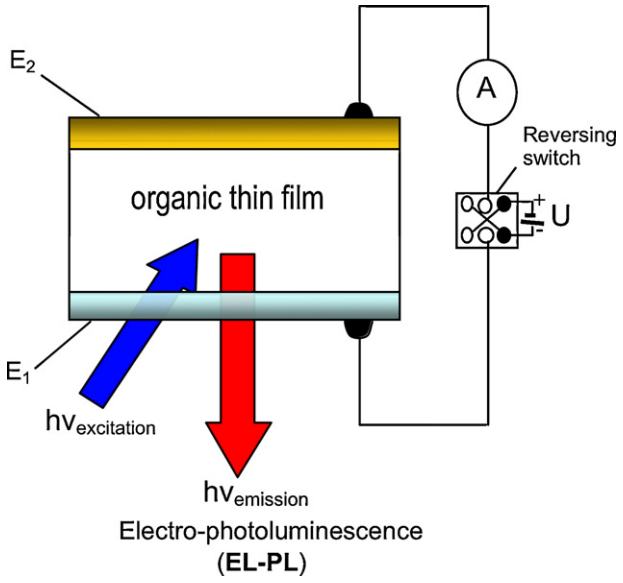

Fig. 25. Electro-photoluminescence (EL-PL) in organic solids. An organic thin film undergoes simultaneous optical ($h\nu_{excitation}$) and electrical (dc voltage U) excitation. The electro-optical characteristics of the EL-PL depend on the charge injection ability and electrical bias of the electrode contacts (E_1, E_2) of which at least one is transparent or semitransparent to light (here electrode E_1).
Reprinted with permission from [101]. ©(2008) Elsevier.

pigments. This plant growth light-emitting LED reveals high efficiency, peaking at 7 μmol s^{-1} W^{-1} for PPF = 1 μmol s^{-1} at 3.5 V, which highly exceeds that for the most recent commercial greenhouse lamps having efficiencies of 1.8 and 1.3 μmol s^{-1} W^{-1} for high-pressure sodium and fluorescent lamps, respectively.

8. Optical switching devices; electro-photoluminescence (EL-PL)

Pt(II) complex-based thin-film structures may also be promising in the preparation of optical switches, that is, devices allowing the mutual control of electrical and optical signals to be employed in a variety of optoelectronic devices. Their function is based on so-called 'electro-photoluminescence' (EL-PL). Its steady-state version discovered recently in organics [103] provides a firm basis for both luminescence-attenuating and -amplifying devices. The EL-PL from an organic thin film structure is illustrated in Fig. 25. The phenomenon involves the combined emission of light from an organic solid film sample excited simultaneously by external radiation (e.g. UV light) and by an applied electric field. The front → ITO excited ($h\nu_{exc}$) photoluminescence (PL) of two electrically polarized organic blend film structures:

(A) $h\nu$ → ITO/m-MTDATA:BPT [1:1] 70 wt%:PC 30 wt% (160 nm)/Ca/Ag
and
(B) $h\nu$ → ITO/m-MTDATA:BPT [1:1] 70 wt%:PtL^2Cl 5 wt%:PC 25 wt% (140 nm)/Ca/Ag

were reported. The molecular structures of the materials used and their energy level diagram, with Fermi level positions indicated for the indium-tin-oxide (ITO) and Ca electrode contacts, are as shown in Fig. 16, along with PL spectra of these two blends and their material components. Unlike the PL component spectra, the emission from the two blends shows up as the broad-band spectrum characteristic of the singlet $^1|$m-MTDATA : BPT$\rangle^*$ and triplet $^3|$m-MTDATA : $PtL^2Cl\rangle^*$ exciplexes, respectively [104]. The EL-PL effect can be observed either as the electric field-induced quenching or enhancement of steady-state total emission for continuous sample excitation conditions. If we define the effective quenching of the total emission output (Φ) as

$$\delta = \frac{\Phi(0) - \Phi(F)}{\Phi(0)} = 1 - \frac{\Phi(F)}{\Phi(0)} \quad (17)$$

where $\Phi(0)$ and $\Phi(F)$ are the total light outputs in the absence and presence of an electric field (F), respectively, we deal with real emission quenching for $\Phi(0) > \Phi(F)$, $\delta > 0$, while $\Phi(0) < \Phi(F)$ leads to negative quenching ($\delta < 0$), that is, to a luminescence enhancement. The measured total emission quenching (TEQ) for samples (A) and (B) is shown as a function of applied field in Fig. 26a. The field evolution of the TEQ (δ) differs according to the electrical bias of the ITO electrode. The monotonous increase of the TEQ observed for the ITO cathode [ITO(−)] (δ^-), changes to a non-monotonous behaviour,

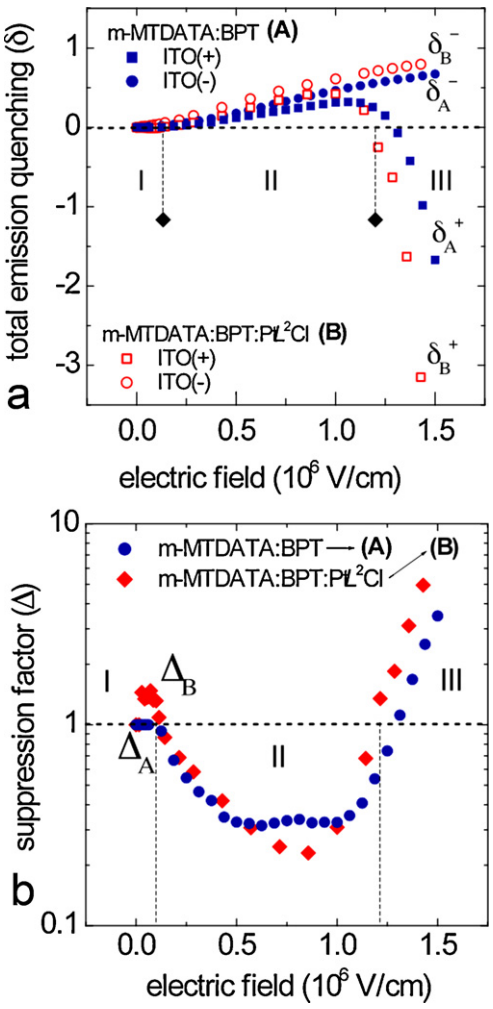

Fig. 26. (a) Measured quenching (δ for the forward and reversed bias of blend A, δ_A^+, δ_A^-, and blend B, δ_B^+, δ_B^-,) of the EL-PL output and (b) its suppression factor (Δ for blend A, Δ_A, and blend B, Δ_B) at varying applied electric field. In contrast to the monotonous increase of quenching for the negatively biased ITO electrode, dramatic quenching roll-off appears reaching high negative values (emission enhancement) at high fields for the positive ITO bias. The presence of the sensitizing phosphor (PtL^2Cl) in blend B leads, in addition, to negative values of δ (emission enhancement) at low electric fields. Three field regions of the TEQ behaviour can apparently be distinguished: Regions I and III of low and high electric fields, respectively, where the total emission enhancement is observed ($\Delta > 1$), and Region II of intermediate electric fields, where the suppression factor falls below 1, indicating the field-induced reduction of the total emission (we note that here the TEQ can be as high as 80%, corresponding to the fractional suppression factor $\Delta_B \approx 0.2$). The wavelength of the exciting light is $\lambda_{exc} = 350$ nm, and its intensity $I_0 = 5 \times 10^{15}$ ph/cm^2 s.
Adapted from [101].

showing a dramatic roll-off down to large negative values at high electric fields for ITO anode [ITO(+)] (δ^+). Relative weakening of TEQ is apparent ($\delta^- > \delta^+$) throughout the overwhelming field range accessible in the experiment with forward-biased structures. This effect can be considered as suppressing the TEQ and characterized by a *suppression factor*

$$\Delta = \frac{\delta^- - \delta^+}{\delta^-} = \frac{\Phi^+(F) - \Phi^-(F)}{\Phi(0) - \Phi^-(F)} \tag{18}$$

The evolution of Δ with applied field for both blends is displayed in Fig. 26b. In addition to Region II representing the efficient reduction in the measured light output quenching ($\Delta < 1$), strong negative quenching ($\Delta > 1$) is observed at high fields (region III). A slight light output enhancement ($\Delta > 1$) is also observed at low electric fields (region I) but only for sample (B) with ITO anode. The ITO(+)/[Ca/Mg(−)] biased film structures act as efficient EL diodes because of the strong injection of holes and electrons at the anode and cathode, respectively, and their recombination in the sample bulk. The charge injection is characterized directly by the dark current. It shows up as the two-orders-of-magnitude larger values of the dark current in the forward-biased samples. Both blends appear highly photoconductive with comparable photocurrents tending to saturation with both forward [ITO(+)] and reversed [ITO(−)] electrode bias [103]. The positive into negative quenching inversion occurs at a field $F = F_{inv}$, where the photocurrent merges with the dark current (cf. Fig. 26). The physical meaning of this coincidence is that the overwhelming part (up to 80%) of the optically excited states undergo quenching by dissociation and/or interaction with space charge [105]. The dissociation of excited species produces the photocurrent tending to saturation. We note that both exciplexes and their donor (m-MTDATA) molecular singlet hot exciton precursors are subject to electron-hole dissociation [104]. The F_{inv} and corresponding current density j ($F = F_{inv}$) vary with characteristics of the exciting light and charge-injection properties of the electrical contacts:

$$j(F_{inv}) \leq \frac{e\alpha I_0 d}{\xi(1-\eta)} \left(1 + \frac{8}{9}\frac{e\mu_e}{\mu_h \eta_{inj}}\right) \tag{19}$$

where μ_e and μ_h are the mobility of electrons and holes, respectively, and $\eta_{inj} = j/j_{SCLC}$ is the carrier-injection efficiency. In general, $\eta_{inj} < 1$ because often the injection current j is lower than the largest injection current density, j_{SCLC}, available under space-charge-limited-current (SCLC) conditions when ohmic electrodes are applied. We note that only a part $(1 - \eta)$ of the excited states participate in the emission since the electric field enhances their dissociation with the efficiency, η. The dissociation takes place either from the emissive exciplex states directly or from their precursors – excited molecular singlet excitons of donor molecules of m-MTDATA (cf., Section 2.2). According to Eq. (19), the current (thus F_{inv}) at which the quenching inversion occurs is expected to increase with increasing optical excitation intensity but decreasing penetration depth of the exciting light. Its value naturally rises with the sample thickness. Indeed, the F_{inv} for thicker sample (A) exceeds that for sample (B) by a factor of 1.14 (see Fig. 26b). One further important conclusion is that j (F_{inv}) increases at decreasing injection efficiency. Since molecules of PtL^2Cl form deep electron traps (see Fig. 16a), the μ_e/μ_h ratio drops down and one would expect $\eta_{inj} \approx 1$ ($j \approx j_{SCLC}$) even at the lowest values of the applied field. A lower field limit of the F_{inv} appears for sample (B) in this case (see Fig. 26b). The upper limit of j (F_{inv}) sets in at high fields, if the field-dependent ratio $\mu_e/\mu_h = f(F)$ increases with electric field and reaches a value sufficient for j to merge with the dark current. We note that, due to the presence of deep electron traps, the ratio μ_e/μ_h is an electric-field-increasing function for fields above 10^5 V/cm.

In summary, there are characteristic field strengths where the quenching switches into enhancement. Their dependence on the illumination conditions and electrical characteristics of such film structures allows, on the one hand, the study of fundamental electronic processes in organic solids and, on the other, the application of the phenomenon to mutual control of electrical and optical signals in a variety of optoelectronic devices. While for non-injecting electrodes (reversed bias), the film structures function as luminescence attenuator devices, charge injection (forward bias) into the films enables their voltage switching from the luminescence-attenuating to -amplifying devices.

9. Concluding remarks

In this review we have sought to give a comprehensive and clearly structured representation of the present state of the development of organic optoelectronic devices based on square-planar, organometallic platinum (II) complexes as light emitters. The understanding and quantitative description of the light emission from thin film multi-layer structures underlying these devices requires detailed knowledge of the function and properties of all their constituents, including charge transport and emissive layers as well as the interfaces between them. Thus, we have given an introduction to organic light emitting devices on the one hand and photophysical characterization of Pt(II) organic complexes as a basis for their emission on the other. By separately describing the possible optoelectronic devices, such as the various classes of OLEDs or optical switches, we have demonstrated the various merits of Pt(II) complexes as light emitters for different applications. One of the most important of them is the very high luminescence quantum yields resulting from cyclometallation and rigid structures, which often lead to a reduction of the rate of non-radiative decay pathways. Another important feature is the propensity of some Pt (II) complexes to form bimolecular excited states such as excimers, electromers, or exciplexes when acting as electron acceptor species, and even more aggregated excited entities. These features, combined with specially designed thin-film layer structures (device architectures) to optimise their performance, clearly allow the fabrication of highly efficient PHOLEDs, NIROLEDs, EXLEDs, WOLEDs or PGOLEDs, of which distinctive examples are described in the present overview.

The performance data of many of these optoelectronic devices are among the best achievements reported for colour and white emission OLEDs and, in some cases, represent top performance parameters. For example, a highest up-to-date external quantum efficiency of 20% (nearly 100% the internal quantum efficiency) has been achieved with a 30–35% PtL^{26}Cl:TCTA blend EML warm-white-light OLED. The top value of CRI (90) has been achieved with a high efficiency WOLED and most efficient EXLED (EL EQE ≈ 2.5%) manufactured employing the PtL^2Cl complex emitter. Furthermore, the highest up-to-date quantum efficiency of NIROLEDs (14.5%) using the same complex as a neat film emitter with a highly electron-injecting electrode PbO_2/Al applied to a four-layer OLED structure has been achieved. It is noteworthy that the observed dependence of the functional shape of the current-density quantum-efficiency evolution on the concentration of Pt(II) complex dopant has allowed the development of a unified approach to modeling EL efficiency in OLEDs. Properties specific to Pt(II) complexes have provided a basis for unique optoelectronic devices, such as PGOLEDs or optical switches described in the present overview.

These examples may suffice to substantiate our conviction that the synthesis of new materials and associated design of optoelectronic devices will continue to establish emissive platinum(II) complexes as distinguished components for green photonics, being

attractive not only in their own right but also as a useful tool for investigating and furthering our understanding of the details of organic electronics.

Organic electronics is making significant inroads into the commercial world. Products based on thin organic film optoelectronic devices are already in the market place. Yet the future holds even greater promise for this technology. Perhaps one of the main limitations at present to further progress and widespread take-up of the technology is the continued high cost of manufacturing of OLEDs. However, the cost of the raw products for their emissive materials, although obviously high in the case of platinum and iridium compounds, does not significantly impact the advancement of OLED technology, owing to the small quantities required. On the contrary, these materials address the critical issue of achieving high quantum efficiency at low voltages, with devices in the offing that perform diverse functions, as exemplified in the present review, which are traditionally accomplished using much more expensive components based on conventional inorganic semiconductor materials.

Acknowledgements

We thank EPRSC for supporting studies of platinum chemistry and organic LEDs based on organometallic Pt(II) complexes, and the members of our research groups who have contributed to some of the developments described above, particularly Drs David Rochester, Lisa Murphy, and Dalia Virgili. The Editor and Professor A. Vlcek are acknowledged for the invitation to contribute a perspective article on these subjects.

References

[1] D. Iams, OIDA Releases New Green Photonics Market Data, www.oida.org/news/oida-news/2008/341 September 10, 2008.
[2] B.W. D'Andrade, S.R. Forrest, Adv. Mater. 16 (2004) 1585.
[3] Universal Display Corporation, Press Releases, 2008 http://www.universaldisplay.com/downloads/Press%20Releases/2008/PANL_whitemilestone_FINAL.pdf.
[4] B.W. D'Andrade, Nat. Photonics 1 (2007) 33.
[5] M. Cocchi, J. Kalinowski, L. Murphy, J.A.G. Williams, V. Fattori, Org. Electron. 11 (2010) 388.
[6] J.A.G. Williams, S. Develay, D.L. Rochester, L. Murphy, Coord. Chem. Rev. 252 (2008) 2596.
[7] J. Kalinowski, J. Phys. D: Appl. Phys. 32 (1999) R179.
[8] J. Kalinowski, Organic Light-emitting Diodes: Principles, Characteristics, and Processes, Marcel Dekker, New York, 2005.
[9] J. Kalinowski, Opt. Mater. 30 (2008) 792.
[10] J. Kalinowski, J. Non-Cryst. Solids 354 (2008) 4170.
[11] J. Kalinowski, M. Cocchi, V. Fattori, L. Murphy, J.A.G. Williams, Org. Electron. 11 (2010) 724.
[12] R. Boyd, Radiometry and the Detection of Optical Radiation, Wiley, New York, 1983.
[13] M.A. Baldo, S.R. Forest, M.E. Thompson, in: Z.H. Kafafi (Ed.), Organic Electroluminescence, Taylor & Francis (CRC), Boca Raton, 2005 (chapter 6).
[14] R.W. Hunt, Measuring Colour, 3rd ed., Fountain Press, England, 1998, ISBN: 0-86343-387-1.
[15] N. Ohta, A.R. Robertson, Colorimetry, Wiley, New York, 2005, pp. 92–96 (chapter 3).
[16] J. Kalinowski, in: Z.H. Kafafi (Ed.), Organic Electroluminescence, Taylor & Francis (CRC), Boca Raton, 2005 (chapter 2).
[17] J. Kalinowski, G. Giro, M. Cocchi, V. Fattori, P. Di Marco, Appl. Phys. Lett. 76 (2000) 2352.
[18] J. Kalinowski, G. Giro, M. Cocchi, V. Fattori, R. Zamboni, Chem. Phys. 277 (2002) 387.
[19] X. Jiang, S. Liu, M.S. Liu, P. Herguth, A.K.-Y. en, H. Fong, M. Sarikaya, Adv. Funct. Mater. 12 (2002) 745.
[20] X. Jiang, R.A. Register, K.A. Killeen, M.E. Thompson, F. Pschenitzka, T.R. Hebner, J.C. Sturm, J. Appl. Phys. 91 (2002) 6717.
[21] J. Kalinowski, in: S. Miyata, H.S. Nalwa (Eds.), Organic Electroluminescent Materials and Devices, Gordon & Breach, Amsterdam, 1997 (chapter 1).
[22] W. Helfrich, in: D. Fox, M.M. Labes, A. Weissberger (Eds.), Physics and Chemistry of the Organic Solid State (vol. 3), Wiley, New York, 1967 (chapter 1).
[23] J. Kalinowski, Synth. Met. 64 (1994) 123.
[24] J. Kalinowski, L.C. Picciolo, H. Murata, Z.H. Kafafi, J. Appl. Phys. 89 (2001) 1866.
[25] J. Kalinowski, H. Murata, L.C. Picciolo, Z.H. Kafafi, J. Phys. D: Appl. Phys. 34 (2001) 3130.
[26] B.W. D'Andrade, S.R. Forrest, J. Appl. Phys. 94 (2003) 3101.
[27] V.I. Adamovich, S.R. Cordero, P.I. Djurovich, A. Tamayo, M.E. Thompson, B.W. D'Andrade, S.R. Forrest, Org. Electron. 4 (2003) 77.
[28] S.-J. Su, E. Gonmori, H. Sasabe, J. Kido, Adv. Mater. 20 (2008) 4189.
[29] C.W. Tang, S.A. VanSlyke, C.H. Chen, J. Appl. Phys. 65 (1989) 3610.
[30] C. Fou, O. Onitsuka, M. Ferreira, M.F. Hubner, B.R. Hsieh, J. Appl. Phys. 79 (1996) 7501.
[31] M.A. Baldo, D.F. O'Brien, Y. You, A. Shoustikov, S. Sibley, M.E. Thompson, S.R. Forrest, Nature (London) 395 (1998) 151.
[32] E.L. Williams, J. Li, G.E. Jabbour, Appl. Phys. Lett. 89 (2006) 083506.
[33] N. Tessler, V. Medvedev, M. Kazes, S. Kan, U. Banin, Science 295 (2002) 1506.
[34] B.W. D'Andrade, R. Holmes, S.R. Forrest, Adv. Mater. 16 (2004) 624.
[35] G. Li, J. Shinar, Appl. Phys. Lett. 83 (2003) 5359.
[36] J. Huang, W.J. Hou, J.H. Li, Y. Yang, Appl. Phys. Lett. 89 (2006) 133509.
[37] S. Reineke, F. Lindner, G. Schwartz, N. Seidler, K. Waltzer, B. Lüssem, K. Leo, Nature (London) 459 (2009) 234.
[38] V. Fattori, J.A.G. Williams, L. Murphy, M. Cocchi, J. Kalinowski, Phot. Nanostr. Fund. Appl. 6 (2008) 225.
[39] G. Parthasarathy, P.E. Burrows, V. Khalfin, V.G. Kozlov, S.R. Forrest, Appl. Phys. Lett. 72 (1998) 2138.
[40] P. Wellenius, A. Suresh, J.F. Muth, Appl. Phys. Lett. 92 (2008) 021111.
[41] L. Flamigni, A. Barbieri, C. Sabatini, B. Ventura, F. Barigelletti, Top. Curr. Chem. 281 (2007) 143.
[42] J.A.G. Williams, Top. Curr. Chem. 281 (2007) 205.
[43] Y. Chi, P.-T. Chou, Chem. Soc. Rev. 39 (2010) 638.
[44] J.A.G. Williams, A.J. Wilkinson, V.L. Whittle, Dalton Trans. (2008) 2081.
[45] S. Lamansky, P. Djurovich, D. Murphy, F. Abdel-Razzaq, H.E. Lee, C. Adachi, P.E. Burrows, S.R. Forrest, M.E. Thompson, J. Am. Chem. Soc. 123 (2001) 4304.
[46] L. Murphy, J.A.G. Williams, Top. Organomet. Chem. 28 (2010) 75.
[47] R. McGuire Jr., M.C. McGuire, D.R. McMillin, Coord. Chem. Rev. 254 (2010) 2574.
[48] P.I. Kvam, M.V. Puzyk, K.P. Balashev, J. Songstad, Acta Chem. Scand. 49 (1995) 335.
[49] J. Brooks, Y. Babayan, S. Lamansky, P.I. Djurovich, I. Tsyba, R. Bau, M.E. Thompson, Inorg. Chem. 41 (2002) 3055.
[50] W.-Y. Wong, C.-L. Ho, J. Mater. Chem. 19 (2009) 4457.
[51] F. Niedermair, O. Kwon, K. Zojer, S. Kappaun, G. Trimmel, K. Mereiter, C. Slugovc, Dalton Trans. (2008) 4006.
[52] B.L. Yin, F. Niemeyer, J.A.G. Williams, J. Jiang, A. Boucekkine, L. Toupet, H. Le Bozec, V. Guerchais, Inorg. Chem. 45 (2006) 8584.
[53] A. Valore, A. Colombo, C. Dragonetti, S. Righetto, D. Roberto, R. Ugo, F. De Angelis, S. Fantacci, Chem. Commun. 46 (2010) 2414.
[54] M. Ghedini, T. Pugliese, M. La Deda, N. Godbert, I. Aiello, M. Amati, S. Belviso, F. Lelj, G. Accorsi, F. Barigelletti, Dalton Trans. 32 (2008) 4303.
[55] J. Liu, C.-J. Yang, Q.-Y. Cao, M. Xu, J. Wang, H.-N. Peng, W.-F. Tan, X.-X. Lue, X.-C. Gao, Inorg. Chim. Acta 362 (2009) 575.
[56] A. Santoro, A.C. Whitwood, J.A.G. Williams, V.N. Kozhevnikov, D.W. Bruce, Chem. Mater. 21 (2009) 3871.
[57] G. Zhou, Q. Wang, X. Wang, C.-L. Ho, W.-Y. Wong, D. Ma, L. Wang, Z. Lin, J. Mater. Chem. 20 (2010) 7472.
[58] G.-J. Zhou, W.-Y. Wong, B. Yao, Z. Xie, L. Wang, J. Mater. Chem. 18 (2008) 1799.
[59] J.-Y. Cho, B. Domercq, S. Barlow, K.Y. Suponitsky, J. Li, T.V. Timofeeva, S.C. Jones, L.E. Hayden, A. Kimyonok, C.R. South, M. Weck, B. Kippelen, S.R. Marder, Organometallics 26 (2007) 4816.
[60] K. Feng, C. Zuniga, Y.-D. Zhang, D. Kim, S. Barlow, S.R. Marder, J.L. Brédas, M. Weck, Macromolecules 42 (2009) 6855.
[61] D.A.K. Vezzu, J.C. Deaton, J.S. Jones, L. Bartolotti, C.F. Harris, A.P. Marchetti, M. Kondakova, R.D. Pike, S. Huo, Inorg. Chem. 49 (2010) 5107.
[62] V. Balzani, V. Carassiti, J. Phys. Chem. 72 (1968) 383.
[63] S.-W. Lai, M.C.-W. Chan, T.-C. Cheung, S.-M. Peng, C.-M. Che, Inorg. Chem. 38 (1999) 4046.
[64] J.A.G. Williams, Chem. Soc. Rev. 38 (2009) 1783.
[65] W. Lu, M.C.-W. Chan, K.-K. Cheung, C.-M. Che, Organometallics 20 (2001) 2477.
[66] W. Lu, B.-X. Mi, M.C.-W. Chan, Z. Hui, C.-M. Che, N. Zhu, S.-T. Lee, J. Am. Chem. Soc. 126 (2004) 4958.
[67] S.J. Farley, D.L. Rochester, A.L. Thompson, J.A.K. Howard, J.A.G. Williams, Inorg. Chem. 44 (2005) 9690.
[68] G.S.-M. Tong, C.-M. Che, Chem. Eur. J. 15 (2009) 7225.
[69] A. Rausch, L. Murphy, J.A.G. Williams, H. Yersin, Inorg. Chem. 48 (2009) 11407.
[70] S. Develay, O. Blackburn, A.L. Thompson, J.A.G. Williams, Inorg. Chem. 47 (2008) 11129.
[71] K.L. Garner, L.F. Parkes, J.D. Piper, J.A.G. Williams, Inorg. Chem. 49 (2010) 476.
[72] S.-Y. Chang, J. Kavitha, J.-Y. Hung, Y. Chi, Y.-M. Cheng, E.-Y. Li, P.-T. Chou, G.-H. Lee, A.J. Carty, Inorg. Chem. 46 (2007) 7064.
[73] J. Rodrigues, L. McDowell, D. Holten, Chem. Phys. Lett. 147 (1988) 235.
[74] J. Kalinowski, W. Stampor, J. Szmytkowski, M. Cocchi, D. Virgili, V. Fattori, P. Di Marco, J. Chem. Phys. 122 (2005) 154710.
[75] M.A. Baldo, C. Adachi, S.H. Forrest, Phys. Rev. B 62 (2000) 10967.
[76] J. Kalinowski, W. Stampor, J. Mezyk, M. Cocchi, D. Virgili, V. Fattori, P. Di Marco, Phys. Rev. B 66 (2002) 235–321.
[77] M. Cocchi, J. Kalinowski, V. Fattori, J.A.G. Williams, L. Murphy, Appl. Phys. Lett. 94 (2009) 073309.
[78] J. Kalinowski, Mater. Sci. -Poland 27 (2009) 735.
[79] M. Cocchi, D. Virgili, C. Sabatini, J. Kalinowski, Chem. Phys. Lett. 421 (2006) 351.

[80] D. Virgili, M. Cocchi, V. Fattori, J. Kalinowski, J.A.G. Williams, Chem. Phys. Lett. 433 (2006) 145.
[81] M. Reufer, M. Walter, P.G. Lagoudakis, A.B. Hummel, J.S. Kolb, H.G. Roskos, U. Scherf, J. Lupton, Nat. Mater. 4 (2005) 340.
[82] S. Difley, D. Beljonne, T. Van Voorhis, J. Am. Chem. Soc. 130 (2008) 3420.
[83] J.B. Birks, Photophysics of Aromatic Molecules, Wiley-Interscience, London, 1970.
[84] Z.-Q. Chen, F. Ding, Z.-Q. Bian, C.-H. Huang, Org. Electron. 11 (2010) 369.
[85] Y. Sun, C. Borek, K. Hanson, P.I. Djurovich, M.E. Thompson, J. Brooks, J. Brown, S.R. Forrest, Appl. Phys. Lett. 90 (2007) 213503.
[86] M. Cocchi, D. Virgili, V. Fattori, J.A.G. Williams,.J. Kalinowski, Appl. Phys. Lett. 90 (2007) 023506.
[87] M. Cocchi, J. Kalinowski, D. Virgili, J.A.G. Williams, Appl. Phys. Lett. 92 (2008) 113302.
[88] T. Jüstel, H. Nikol, C. Ronda, Angew. Chem. Int. Ed. 37 (1998) 3084.
[89] J. Kido, M. Kimura, K. Nagai, Science 267 (1995) 1332.
[90] Y.-S. Park,.-W. Kang, D.M. Kang, J.-W. Park, Y.-H. Kim, S.-K. Kwon, J.-J. Kim, Adv. Mater. 20 (2008) 1957.
[91] P.E. Burrows, V. Khalfin, G. Gu, S.R. Forest, Appl. Phys. Lett. 73 (1998) 435.
[92] Y. Sun, N.C. Giebink, H. Kanno, B. Ma, M.E. Thompson, S.R. Forrest, Nature 440 (2006) 908.
[93] J. Kido, K. Hongawa, K. Okuyama, K. Nagai, Appl. Phys. Lett. 64 (1994) 815.
[94] B.W. D'Andrade, R.J. Holmes, S.R. Forrest, Adv. Mater. 16 (2004) 624.
[95] Y.-H. Niu, M.S. Liu, J.-W. Ka, J. Bardeker, M.T. Zin, R. Schofield, Y. Chi, A.K.-Y. Jen, Adv. Mater. 19 (2007) 300.
[96] E.L. Williams, K. Haavisto, J. Li, G.E. Jabbour, Adv. Mater. 19 (2007) 197.
[97] D. Wang, W. Lu, Z.S. Su, T.L. Li, B. Chu, D.F. Bi, L.L. Chen, W.M. Su, H. He, Appl. Phys. Lett. 89 (2006) 233511.
[98] V. Adamovich, J. Brooks, A. Tamayao, A.M. Alexander, P.I. Djurovich, B.W. D'Andrade, C. Adachi, S.R. Forrest, M.E. Thompson, New J. Chem. 26 (2002) 1171.
[99] M. Cocchi, J. Kalinowski, D. Virgili, V. Fattori, S. Develay, J.A.G. Williams, Appl. Phys. Lett. 90 (2007) 163508.
[100] J. Kalinowski, M. Cocchi, D. Virgili, V. Fattori, J.A.G. Williams, Adv. Mater. 19 (2007) 4000.
[101] B.W. D'Andrade, J. Brooks, V. Adamovich, M.E. Thompson, S.R. Forrest, Adv. Mater. 14 (2002) 1032.
[102] G.S. Singhal, et al. (Eds.), Concepts in Photobiology: Photosynthesis and Photomorphogenesis 11–15, Narosa Publishing House, 1999.
[103] J. Kalinowski, M. Cocchi, D. Virgili, V. Fattori, J.A.G. Williams, Chem. Phys. Lett. 447 (2007) 279.
[104] J. Kalinowski, M. Cocchi, D. Virgili, V. Fattori, J.A.G. Williams, Chem. Phys. Lett. 432 (2006) 110.
[105] J. Kalinowski, M. Cocchi, D. Virgili, C. Sabatini, Appl. Phys. Lett. 89 (2006) 011105.